Diagnosing the radiation biases in global climate models using radiative kernels

Han Huang[1] and Yi Huang[2]

[1]Department of Atmospheric and Oceanic Sciences, McGill University
[2]McGill University

March 26, 2023

Abstract

Radiation energy balance at the top of the atmosphere (TOA) is a critical boundary condition for the Earth climate. It is essential to validate it in the global climate models (GCM) on both global and regional scales. However, the comparison of overall radiation field is known to conceal compensating errors. Here we use a new set of radiative kernels to diagnose the radiation biases by different geophysical variables in the latest GCMs. We find although clouds remain a primary cause of radiation biases, the radiation biases caused by non-cloud variables are of comparable magnitudes. Many GCMs tend to have a cold bias in the air temperature and a moist bias in the tropospheric humidity, which lead to considerable biases in TOA radiation budget but are compensated by cloud biases. These findings signify the importance of validating the GCM-simulated radiation fields, with respect to both the overall and component radiation biases.

Diagnosing the radiation biases in global climate models using radiative kernels

Han Huang, Yi Huang

Department of Atmospheric and Oceanic Sciences, McGill University, Montreal, Canada

Corresponding Authors:

Yi Huang, yi.huang@mcgill.ca (ORCID: 0000-0002-5065-4198)

Abstract

Radiation energy balance at the top of the atmosphere (TOA) is a critical boundary condition for the Earth climate. It is essential to validate it in the global climate models (GCM) on both global and regional scales. However, the comparison of overall radiation field is known to conceal compensating errors. Here we use a new set of radiative kernels to diagnose the radiation biases by different geophysical variables in the latest GCMs. We find although clouds remain a primary cause of radiation biases, the radiation biases caused by non-cloud variables are of comparable magnitudes. Many GCMs tend to have a cold bias in the air temperature and a moist bias in the tropospheric humidity, which lead to considerable biases in TOA radiation budget but are compensated by cloud biases. These findings signify the importance of validating the GCM-simulated radiation fields, with respect to both the overall and component radiation biases.

(Plain Language Abstract)

Radiation energy balance at the top of atmosphere is crucial to the Earth climate system and is routinely examined in climate model validations. Here, we show that seemingly good agreements between model and observation can be due to compensating errors and propose the use of a kernel method for separately identifying component radiation biases due to different geophysical variables, which may afford a more stringent test of climate models.

Key Points

1. Climate models are subject to compensating radiation biases caused by cloud and non-cloud variables.
2. Many models have a cold temperature bias and a moist humidity bias in the troposphere.
3. Kernel diagnosis of component radiation biases affords a stricter test for climate models.

1. Introduction

Radiation energy balance at the top of the atmosphere (TOA) critically shapes the Earth climate. The global mean values of the longwave and shortwave radiation fluxes, as well as their distribution patterns are often used to validate the simulations of the global climate models (GCMs) (e.g., Kiehl et al. 1994; Su et al. 2010; Li et al. 2013; Dolinar et al. 2015; Loeb et al. 2020; Wild 2020). As illustrated by Fig. 1 (a) to (f) and also by others (e.g., Zhao et al. 2018; Golaz et al. 2019), the state-of-the-art GCMs show remarkable skills in reproducing observed climatological mean radiation fields, including the net radiation and its longwave and shortwave components.

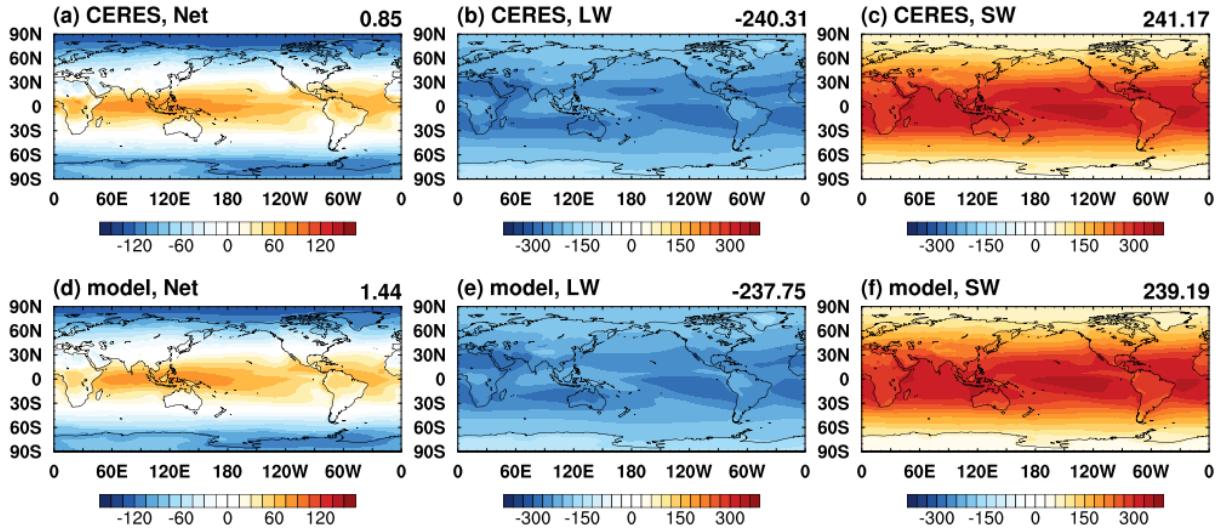

Figure 1. Climatological mean radiative fluxes in all-sky (units: W m^{-2}) from (a, b, c) the CERES satellite observation, and (d, e, f) multi-model mean of the AMIP simulations of GCMs. Global mean values are shown on the upper-right corner in each panel. AMIP: Atmospheric Modelling Intercomparison Project; GCM: Global Climate Model; CERES: Clouds and the Earth's Radiant Energy System.

However, the validation of GCMs with regard to overall radiation field is known to conceal possible compensating errors (Huang et al. 2007; Huang and Ramaswamy 2008; Huang, X. et al. 2008, 2013; Bani Shahabadi et al. 2016; Della Fera et al. 2022). For example, Huang et al. (2007) showed, by validating a GCM against spectrally resolved satellite radiance, that a seemingly good all-sky OLR field may result from compensating radiation errors due to the biases in the cloud fields and those in the non-cloud fields, such as the atmospheric temperature and humidity. On the other hand, comparisons of geophysical variables between GCM simulations and observations, such as the satellite retrieval products, verify the biases in the non-radiation fields. Some of these biases, such as those in the tropospheric humidity and temperature, appear to be persistent in a number of models (Gettelman et al. 2006, Jiang et al. 2015). These recognitions thus bear important questions: Is the agreement in the radiation fields between the latest GCMs and observations, as shown in Fig. 1, subject to compensating errors? And how much do different geophysical variables respectively contribute to the total radiation bias?

To answer the above questions, especially the latter one, it is important to have a comprehensive view of the error budget of the radiation fields and the ability to identify the biases that matter the most energetically. Among the potential causes of radiation errors, clouds are broadly conceived to be a major source of uncertainty in GCM simulations. This can and should be confirmed by quantifying the cloud-induced radiation bias and compare it to those caused by other geophysical variables. If, as revealed by previous studies (e.g., Huang et al. 2007), the cloud fields were tuned to compensate non-cloud biases in order for the model-simulated all-sky radiation to match the observation, the model would have cloud and non-cloud radiation biases of comparable magnitudes and opposite signs. On a relevant note, radiation biases are often cited to justify the need of treating certain processes in the GCMs. A recent example is the inclusion of the longwave scattering effect of clouds in the radiation codes (e.g., Chen et al. 2020). However, the impact of a proposed modification cannot be properly expected without a "big-picture" knowledge, i.e., what other, possibly more dominant, radiation biases exist in the models. These issues emphasize the need to separately quantify the individual radiation biases. This is important to verify that the radiation agreement in a model is achieved for the right reasons, or to identify which variable fields or physical processes are the most imperative to improve.

In this paper, we use a radiative kernel method to quantify the radiative biases caused by different geophysical variables, including surface and atmospheric temperature, humidity, surface albedo and clouds. The method and data are presented in Section 2. A systematic assessment of the radiative biases in the current GCMs is shown in Section 3.

2. Method

2.1 Observation and GCM data

To quantify the biases in the GCM-simulated radiation fields, we use the satellite observation of the Clouds and the Earth's Radiant Energy System (CERES, Wielicki et al., 1996) as the reference values of the TOA radiation fluxes. Specifically, its Energy Balanced and Filled (EBAF) dataset, version 4.2, with clear-sky radiation value consistently defined as in the GCMs (Loeb et al. 2018, 2020) is used. All the radiative fluxes are defined to be downward positive.

To quantify the GCM biases in the geophysical variables, we use the fifth generation European Centre for Medium-Range Weather Forecasts atmospheric reanalysis (ERA5) (Hersbach et al., 2020) as the reference values of such variables as surface and atmospheric temperature, water vapor, surface albedo.

The GCMs examined here are the models of the sixth phase of the Coupled Model Intercomparison Project (CMIP6, Eyring et al., 2016). Particularly, the Atmospheric Modelling Intercomparison Project (AMIP) simulations of the same period as the CERES data, years 2001-2014, are used here for analysis. A list of the models included in this analysis are summarized in the Supplementary Table S1.

2.2 Quantification of component biases: Kernel method

Radiative kernels, $\frac{\partial R}{\partial x}$, are pre-calculated radiative sensitivities to different geophysical variables, x, including surface temperature, atmospheric temperature and water vapor at different altitudes, and surface albedo. In this work, we use the radiative kernels computed by Huang & Huang (2023, under review) based on the ERA5 global reanalysis dataset. When multiplied by an anomaly of the geophysical variable, Δx, the product measures the radiation difference due to this anomaly:

$$\Delta R_x = \frac{\partial R}{\partial x}\Delta x \qquad (1)$$

Consider Δx to be the bias of the geophysical variable x with respect to a reference value, which we take from ERA5 reanalysis of the same period in this study; then the above equation measures radiative bias caused by x, which is a main objective here. The multi-model mean biases in the geophysical variables are shown in Supplementary Information (Fig. S1).

Radiative kernels have been widely used for radiative analyses, e.g., for quantifying climate feedbacks (e.g., Soden & Held 2006, Shell et al. 2008). A known limitation of Equation (1) is that it cannot be readily applied to cloud property variables whose effects on the radiation fields are strongly nonlinear. Hence, adopting the adjusted cloud radiative effect method used in feedback analysis (Shell et al. 2008), we measure the cloud-induced radiative bias essentially as a residual effect:

$$\Delta R_C = (\Delta R - \Delta R^0) - \sum_x (\Delta R_x - \Delta R_x^0) \qquad (2)$$

Here, ΔR and ΔR^0 are the all-sky and clear-sky total radiative biases in any of the TOA radiation fluxes: longwave (LW), shortwave (SW) or Net (LW+SW). ΔR_x and ΔR_x^0 are the all-sky and clear-sky component radiative biases caused by a non-cloud geophysical variable, as measured by Equation (1). Note the first term on the right-hand side of Equation (2) is the model bias in cloud radiative effect (CRE),

$$\Delta CRE = \Delta(R - R^0) \qquad (3)$$

which is often used to measure cloud-induced radiation bias but as discussed in the *Results* section is subject to errors.

As we use different datasets as the references of radiation fluxes (CERES) and geophysical variables (ERA5), it is worth examining their consistency. The Supplementary Fig. S2 shows the radiation biases of CMIP6 models against CERES and ERA5 are similar. Together with the radiation closure tests presented below, which verifies that the total bias ΔR can be explained by the sum of the component biases $\sum \Delta R_x$, this verifies the validity of using the geographical variables from ERA5 to diagnose the radiation biases against CERES.

3. Results

3.1 Global mean total radiation bias

According to the CERES data, the global annual mean all-sky longwave and shortwave radiation fluxes for the period of 2001-2014 are 240.31 and 241.17 W m^{-2}, respectively. As summarized in Table 1 and illustrated by Fig. 1, the CMIP6 models generally well reproduce these radiation fluxes, with multi-model mean biases in the global mean values being 2.57 and -1.97 W m^{-2} (in the order of 1%) and the root-mean-squares (RMS, which measure the magnitude of the biases regardless of their signs) being 3.89 and 4.20 W m^{-2}; see Supplementary Table S1 and S2 for the biases in the individual models.

		All-sky			Clear-sky		
		Longwave	Shortwave	Net	Longwave	Shortwave	Net
CERES observation		-240.31	241.17	0.85	-266.29	286.61	20.32
	Overall radiation biases (model minus observation)						
CMIP6 model bias	mean	2.57	-1.97	0.59	3.99	0.98	4.97
	RMS	3.89	4.20	2.32	4.68	2.54	6.35
	Kernel-diagnosed component radiation biases						
total bias	mean	1.58	-2.50	-0.92	3.00	0.45	3.46
	RMS	3.48	3.96	2.97	3.84	2.25	5.22
Surface (land) temperature	mean	-0.17	---	-0.17	-0.26	---	-0.26
	RMS	0.31		0.31	0.45		0.45
Atmospheric temperature	mean	1.78	---	1.78	1.62	---	1.62
	RMS	2.66		2.66	2.44		2.44
Water vapor	mean	1.31	0.19	1.50	1.64	0.09	1.73
	RMS	2.00	0.27	2.26	2.52	0.14	2.66
Surface albedo	mean	---	0.42	0.42	---	0.37	0.37
	RMS		1.74	1.74		2.20	2.20
Cloud	mean	-1.34	-3.11	-4.45	---	---	---
	RMS	2.88	5.04	5.24			
Residual	mean	0.98	0.53	1.51	0.98	0.53	1.51
	RMS	2.20	1.86	2.87	2.20	1.86	2.87

Table 1. The radiation biases in the CMIP6 models. Units: W m^{-2}. Summarized in this table are the multi-model mean and root-mean-square (RMS) of the biases in the global mean radiation fluxes of all the models examined (their respective biases are documented in Supplementary Tables S1 and S2).

Although the CMIP6 GCMs generally achieve excellent accuracy in their simulations of the all-sky global mean radiation budget, it is interesting to note that many of these models have larger clear-sky global mean biases than the all-sky ones. For the global mean TOA net radiation (the sum of longwave and shortwave fluxes) as an example, the RMS biases are 2.32 W m^{-2} in the all-sky and 6.35 W m^{-2} in the clear-sky. These results indicate that compensating errors caused by cloud and non-cloud variables noted in earlier studies (e.g., Huang et al. 2007) still exist in the current models. If a GCM has biases in non-cloud variables (as indicated by clear-sky radiation biases), when its cloud fields are tuned to match the observed all-sky radiation values,

it will have to produce cloud biases to offset non-cloud biases, to achieve a seeming agreement with the observations. This means that besides the cloud biases that are widely recognized and often emphasized, it is equally important to address the radiation biases due to non-cloud variables, to simulate a truly correct radiation budget in the GCMs.

Moreover, as illustrated by the standard deviation of the model biases in Table S3, the relative biases between the GCMs are of similar magnitudes to the multi-model mean and RMS biases. This aspect of the model bias is independent of the choice of truth reference (for which the CERES dataset is used in this study).

3.2 Component radiation bias

The diagnosis above signifies the importance of quantifying the radiation biases induced by different geophysical variables individually. Here, we use the kernel method described in Section 2.2 to measure the component radiation biases caused by each of these variables: surface temperature, atmospheric temperature, water vapor, surface albedo and cloud. It is worth noting that although the GCMs can generally well reproduce the global mean radiation budget compared to CERES, there exist regional biases of greater magnitudes, which as revealed below can be an order of magnitude larger than the global mean biases. It is thus important to examine the component radiation bias at both global and regional scales.

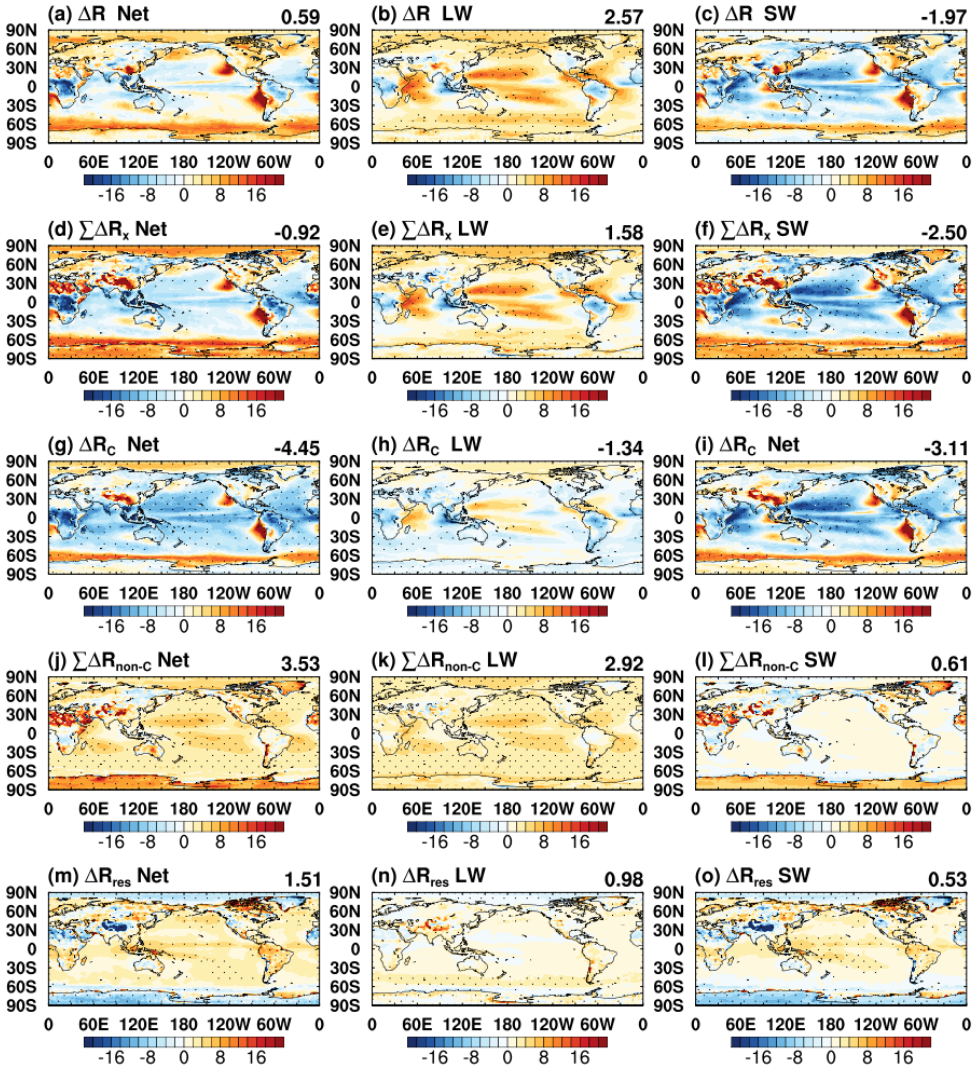

Figure 2. The multi-model mean total and component all-sky radiation biases in the CMIP6 models; units: W m^{-2}. Shown in the three columns are the Net, longwave and shortwave biases, respectively. Shown in the different rows are ΔR: the total bias, $\sum \Delta R_x$: the sum of all the component biases diagnosed from the kernel method, ΔR_C: the radiation bias due to cloud, ΔR_{non-C}: the radiation bias due to non-cloud variables, and ΔR_{res}: the unexplained bias residual. The dotted areas indicate where the multi-model mean bias is larger than the standard deviation.

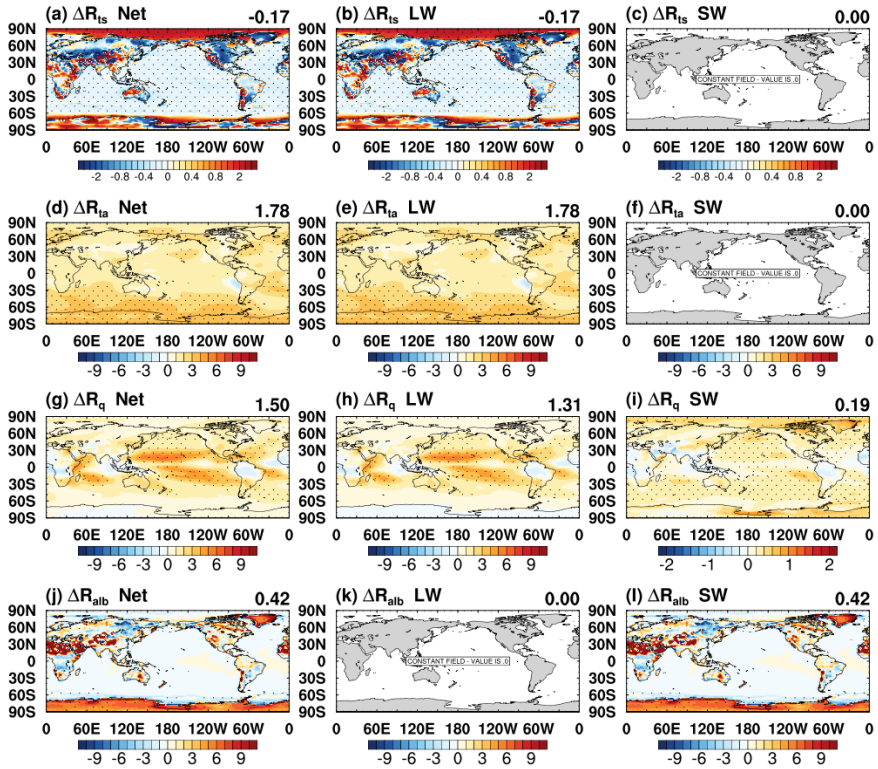

Figure 3. Like Figure 2, but for component radiation biases diagnosed by the kernel method. Shown in the different rows in order are the biases by surface temperature (ΔR_{ts}), air temperature (ΔR_{ta}), water vapor (ΔR_q), and surface albedo (ΔR_{alb}).

Fig. 2 and 3 show the global distributions of the total and component radiation biases averaged from all the models examined here; it complements the global mean bias values summarized in Table 1. In addition, interested readers can find the spatial correlation between the component and total radiation biases in the Supplementary Table S4 and S5, the distributions of the multi-model mean clear-sky biases in Figures S3 and S4, and the component radiation biases in each model in the Supplementary datafile.

The results in Fig. 2 affirm that kernel-diagnosed radiation biases ($\sum \Delta R_x$) can explain the majority of the total radiation biases (ΔR) in GCMs; their spatial correlations are 0.84, 0.69 and 0.70 for the longwave, shortwave and net radiation, respectively; the performance as measured by spatial correlation for each model is documented in Supplementary Table S4 and S5. The generally small residuals ($\Delta R_{res} = \Delta R - \sum \Delta R_x$) indicate that the kernel method achieves a good radiation closure in explaining the total ΔR, especially for the longwave radiation budget.

Cloud-induced radiation biases are well recognized to be a primary contributor to the total radiation biases. Table 1 and Fig. 2 (g-i) show that it has the largest global mean biases, as well as prominent regional biases, which explain most of the spatial variance of the total biases (see the spatial correlation coefficients in Supplementary Table S4, which is typically about 0.8). Using the RMS of bias values in every grid point, we find the all-sky spatial biases in the CMIP6 models are typically in the order of several W m^{-2}, although some models have larger values exceeding 10 W m^{-2} (see Supplementary Table S6), which are mainly contributed by the cloud

biases. The cloud biases are noticeably larger in the shortwave than in the longwave, as shown by the multi-model mean in Fig. 2, which shows local maxima exceeding 15 W m $^{-2}$ (the maximum biases in the individual models may exceed 50 W m $^{-2}$). We find strong, common biases in the stratocumulus regions in the eastern side of the ocean basins, e.g., adjacent to the coasts of California and Peru, where considerably less solar radiation is reflected by the modelled clouds compared to the CERES observation. In the rest of the tropical ocean, modelled clouds tend to be too reflective. These shortwave biases are offset to some extent by the longwave cloud biases, due to the compensating nature of cloud radiative effects.

We also find significant biases caused by the non-cloud variables. Some of them have global mean magnitudes comparable to the cloud biases (Table 1). In particular, we find that many models have a cold bias in the air temperature and moist bias in the water vapor concentration in the troposphere (see Fig S1), both of which lead to an underestimation of the outgoing longwave radiation - a positive bias in terms of TOA radiation budget (downward positive). As marked by the shaded areas in Fig. 3 (d) and (g), the water vapor bias and air temperature bias lead to radiation biases in many models in Tropical Pacific and Southern Oceans, respectively. Interestingly, these positive non-cloud biases tend to be compensated by cloud biases of an opposite sign, which in some models results in a seemingly good all-sky radiation budget (see Tables 1 and S1) as noted above.

It is worth noting that cloud bias is often measured by the cloud radiative effect (ΔCRE, as given in Equation (3)). Because this quantity depends on the clear-sky radiation field, this potentially aliases model errors in clear-sky radiation fields caused by the non-cloud variables as cloud bias. In comparison, the cloud bias ΔR_C measured by Equation (2) explicitly deducts the contributions from non-cloud variables to the total radiation bias (ΔR) and thus is less subject to such aliasing errors. Comparing ΔR_C and ΔCRE in the CMIP6 GCMs, we find that except in several models (see Supplementary Table S1), the two measures agree to within 10% in terms of global mean cloud biases. However, as illustrated by Supplementary Fig. S5, in some models and especially in regions where non-cloud biases prevail such as in the Arctic, the use of ΔCRE can strongly bias the measure of cloud radiative bias.

4. Discussions and Conclusions

In this paper, we propose and demonstrate the use of radiative sensitivity kernels for diagnosing the radiation biases in the GCMs. Using this method, we assess the TOA radiation fluxes simulated in the AMIP runs of the CMIP6 climate models against the CERES satellite observations and quantify how the total model biases in the net, longwave and shortwave radiation fields result from the biases in their geophysical variables, including surface temperature and albedo, atmospheric temperature and water vapor concentration, and cloud.

In terms of global mean radiation fluxes, the CMIP6 models can well reproduce the CERES-observed all-sky values. However, we find many of the models have larger biases in the clear-sky global mean radiation budget, with the biases in the net radiation fluxes typically amounting to several W m^{-2} and being several times of their all-sky values (Tables 1 and S1). This signifies the existence of compensating errors in their simulated radiation fields.

Specifically, cloud biases, possibly due to model tuning, compensate the radiation biases caused by non-cloud variables.

Cloud-induced radiation bias makes a primary contribution to the total radiation bias. This is especially the case for the shortwave radiation field, where significant biases are found in the tropical regions, signifying errors in cloudiness and thus reflected solar radiation.

Concerning the non-cloud biases, we find that many models have a cold bias in the air temperature and a moist bias in the tropospheric humidity compared to the ERA5 reanalysis. These biases each lead to a global mean radiation bias in the magnitude of several W m^{-2} (Tables 1 and S1), and persistent regional biases especially in the Tropical and middle-latitude oceans (Fig. 3). This means that the GCMs cannot achieve a good (better than several W m^{-2}) radiation closure compared to the observation benchmarks without addressing these non-cloud biases.

The kernel method used here aims to obtain a first-order quantification of the component radiation biases. Given its linear approximation nature (Equation (1)), it is inevitable to leave residuals in the model error budget. Moreover, the uncertainty of greenhouse gas and aerosols prescribed in the models may also contribution to the residuals. Nevertheless, the explained bias ($\sum \Delta R_x$) is generally strongly spatially correlated with the total flux biases (ΔR) (see Table S4 and S5), indicating the method can explain the majority of model biases. Another notable strength of it is that it avoids the aliasing issue in quantifying the cloud radiative bias. The significant component biases, namely the cloud, air temperature and tropospheric humidity biases, disclosed by this method warrant further investigations.

Acknowledgements

We thank Yuwei Wang and Jing Feng for their helpful comments. We acknowledge the grants from the Natural Sciences and Engineering Research Council of Canada (RGPIN-2019-04511) and the Fonds de Recherché Nature et Technologies of Quebec (2021-PR-283823) that supported this research.

Data Availability Statement

The ERA5 datasets can be accessed through the ECMWF website (C3S, 2017). The ERA5-based radiative kernels can be downloaded at H. Huang (2023a). The kernel-diagnosed total and component radiation biases in all the CMIP6 models examined here can be obtained from: H. Huang (2023b).

References

Bani Shahabadi, M., Huang, Y., Garand, L., Heilliette, S., and Yang, P. (2016), Validation of a weather forecast model at radiance level against satellite observations allowing quantification of temperature, humidity, and cloud-related biases, *J. Adv. Model. Earth Syst.*, 8, 1453– 1467, doi:10.1002/2016MS000751.

Chen, Y. H., Huang, X., Yang, P., Kuo, C. P., & Chen, X. (2020). Seasonal dependent impact of ice cloud longwave scattering on the polar climate. *Geophysical Research Letters*, 47(23), e2020GL090534.

Copernicus Climate Change Service (C3S) (2017). ERA5 [Dataset]: Fifth generation of ECMWF atmospheric reanalyses of the global climate . Copernicus Climate Change Service Climate Data Store (CDS), date of access. https://cds.climate.copernicus.eu/cdsapp#!/home

Della Fera, S., Fabiano, F., Raspollini, P., Ridolfi, M., Cortesi, U., Barbara, F., and von Hardenberg, J. (2022) On the use of IASI spectrally resolved radiances to test the EC-Earth climate model (v3.3.3) in clear-sky conditions, EGUsphere [preprint], https://doi.org/10.5194/egusphere-2022-479.

Dolinar, E.K., Dong, X., Xi, B. et al. Evaluation of CMIP5 simulated clouds and TOA radiation budgets using NASA satellite observations. Clim Dyn 44, 2229–2247 (2015). https://doi.org/10.1007/s00382-014-2158-9

Eyring, V., Bony, S., Meehl, G. A., Senior, C. A., Stevens, B., Stouffer, R. J., & Taylor, K. E. (2016). Overview of the Coupled Model Intercomparison Project Phase 6 (CMIP6) experimental design and organization. *Geoscientific Model Development*, 9(5), 1937-1958.

Golaz, J. C., Caldwell, P. M., Van Roekel, L. P., Petersen, M. R., Tang, Q., Wolfe, J. D., ... & Zhu, Q. (2019). The DOE E3SM coupled model version 1: Overview and evaluation at standard resolution. *Journal of Advances in Modeling Earth Systems*, 11(7), 2089-2129. https://doi.org/10.1029/2018MS001603

Gettelman, A., Collins, W. D., Fetzer, E. J., Eldering, A., Irion, F. W., Duffy, P. B., & Bala, G. (2006). Climatology of Upper-Tropospheric Relative Humidity from the Atmospheric Infrared Sounder and Implications for Climate, *Journal of Climate*, *19*(23), 6104-6121. https://journals.ametsoc.org/view/journals/clim/19/23/jcli3956.1.xml

Hersbach, H., Bell, B., Berrisford, P., Hirahara, S., Horányi, A., Muñoz-Sabater, J., Schepers, D. (2020). The ERA5 global reanalysis. Quarterly Journal of the Royal Meteorological Society, 146(730), 1999-2049.

Huang, Han (2023a), “Data for ERA5 radiative kernels”, Mendeley Data, V2, doi: 10.17632/vmg3s67568.2

Huang, Han (2023b), “Data for "diagnosing the radiation biases in the global climate models using relative kernels"”, Mendeley Data, V2, doi: 10.17632/6j5999szj6.2

Huang, H., & Huang, Y. (2023). Radiative sensitivity quantified by a new set of radiation flux kernels based on the ERA5 reanalysis, *Earth System Science Data*, (under review).

Huang, X., Yang, W., Loeb, N. G., and Ramaswamy, V. (2008), Spectrally resolved fluxes derived from collocated AIRS and CERES measurements and their application in model evaluation: Clear sky over the tropical oceans, *J. Geophys. Res.*, 113, D09110, doi:10.1029/2007JD009219.

Huang, X., Cole, J. N. S., He, F., Potter, G. L., Oreopoulos, L., Lee, D., Suarez, M., & Loeb, N. G. (2013). Longwave Band-By-Band Cloud Radiative Effect and Its Application in GCM Evaluation, *Journal of Climate*, *26*(2), 450-467. Retrieved Sep 13, 2022, from https://journals.ametsoc.org/view/journals/clim/26/2/jcli-d-12-00112.1.xml

Huang, Y., Ramaswamy, V., Huang, X., Fu, Q., and Bardeen, C. (2007), A strict test in climate modeling with spectrally resolved radiances: GCM simulation versus AIRS observations, *Geophys. Res. Lett.*, 34, L24707, doi:10.1029/2007GL031409.

Huang, Y., & Ramaswamy, V. (2008). Observed and simulated seasonal co-variations of outgoing longwave radiation spectrum and surface temperature. *Geophys. Res. Lett.*, 35(17).

Jiang, J. H., Su, H., Zhai, C., Wu, L., Minschwaner, K., Molod, A. M., and Tompkins, A. M. (2015), An assessment of upper troposphere and lower stratosphere water vapor in MERRA, MERRA2, and ECMWF reanalyses using Aura MLS observations, *J. Geophys. Res. Atmos.*, 120, 11,468– 11,485, doi:10.1002/2015JD023752.

Kato, S., Rose, F. G., Rutan, D. A., Thorsen, T. J., Loeb, N. G., Doelling, D. R., Huang, X., Smith, W. L., Su, W., & Ham, S. (2018). Surface Irradiances of Edition 4.0 Clouds and the Earth’s Radiant Energy System (CERES) Energy Balanced and Filled (EBAF) Data Product, Journal of Climate, 31(11), 4501-4527.

Kiehl, J. T., Hack, J. J., and Briegleb, B. P. (1994), The simulated Earth radiation budget of the National Center for Atmospheric Research community climate model CCM2 and comparisons with the Earth Radiation Budget Experiment (ERBE), J. Geophys. Res., 99(D10), 20815–20827, doi:10.1029/94JD00941.

Li, J.-L. F., Waliser, D. E., Stephens, G., Lee, S., L'Ecuyer, T., Kato, S., Loeb, N., and Ma, H.-Y. (2013), Characterizing and understanding radiation budget biases in CMIP3/CMIP5 GCMs, contemporary GCM, and reanalysis, J. Geophys. Res. Atmos., 118, 8166– 8184, doi:10.1002/jgrd.50378.

Loeb, N. G., Doelling, D. R., Wang, H., Su, W., Nguyen, C., Corbett, J. G., Liang, L., Mitrescu, C., Rose, F. G., & Kato, S. (2018). Clouds and the Earth’s Radiant Energy System (CERES)

Energy Balanced and Filled (EBAF) Top-of-Atmosphere (TOA) Edition-4.0 Data Product, Journal of Climate, 31(2), 895-918.

Loeb, N. G., Rose, F. G., Kato, S., Rutan, D. A., Su, W., Wang, H., Doelling, D. R., Smith, W. L., & Gettelman, A. (2020). Toward a Consistent Definition between Satellite and Model Clear-Sky Radiative Fluxes, *Journal of Climate*, *33*(1), 61-75.

Shell, K. M., Kiehl, J. T., & Shields, C. A. (2008). Using the radiative kernel technique to calculate climate feedbacks in NCAR's Community Atmospheric Model. *Journal of Climate*, 21(10), 2269-2282.

Soden, B. J., & Held, I. M. (2006). An assessment of climate feedbacks in coupled ocean–atmosphere models. *Journal of climate*, 19(14), 3354-3360.

Su, W., Bodas-Salcedo, A., Xu, K.-M., and Charlock, T. P. (2010), Comparison of the tropical radiative flux and cloud radiative effect profiles in a climate model with Clouds and the Earth's Radiant Energy System (CERES) data, J. Geophys. Res., 115, D01105, doi:10.1029/2009JD012490.

Wielicki, B. A., B. R. Barkstrom, E. F. Harrison, R. B. Lee III, G. L. Smith, and J. E. J. B. o. t. A. M. S. Cooper (1996), Clouds and the Earth's Radiant Energy System (CERES): An earth observing system experiment, B Am Meteorol Soc, 77(5), 853-868.

Wild, M. (2020). The global energy balance as represented in CMIP6 climate models. *Clim Dyn* **55**, 553–577. https://doi.org/10.1007/s00382-020-05282-7

Zhao, M., Golaz, J.-C., Held, I. M., Guo, H., Balaji, V., Benson, R., et al. (2018). The GFDL global atmosphere and land model AM4.0/LM4.0: 1. Simulation characteristics with prescribed SSTs. *Journal of Advances in Modeling Earth Systems*, 10, 691– 734. https://doi.org/10.1002/2017MS001208

Zhang, M. H., Lin, W. Y., and Kiehl, J. T. (1998), Bias of atmospheric shortwave absorption in the NCAR Community Climate Models 2 and 3: Comparison with monthly ERBE/GEBA measurements, J. Geophys. Res., 103(D8), 8919– 8925, doi:10.1029/98JD00343.

Diagnosing the radiation biases in global climate models using radiative kernels

Han Huang, Yi Huang

Department of Atmospheric and Oceanic Sciences, McGill University, Montreal, Canada

Corresponding Authors:

Yi Huang, yi.huang@mcgill.ca (ORCID: 0000-0002-5065-4198)

Abstract

Radiation energy balance at the top of the atmosphere (TOA) is a critical boundary condition for the Earth climate. It is essential to validate it in the global climate models (GCM) on both global and regional scales. However, the comparison of overall radiation field is known to conceal compensating errors. Here we use a new set of radiative kernels to diagnose the radiation biases by different geophysical variables in the latest GCMs. We find although clouds remain a primary cause of radiation biases, the radiation biases caused by non-cloud variables are of comparable magnitudes. Many GCMs tend to have a cold bias in the air temperature and a moist bias in the tropospheric humidity, which lead to considerable biases in TOA radiation budget but are compensated by cloud biases. These findings signify the importance of validating the GCM-simulated radiation fields, with respect to both the overall and component radiation biases.

(Plain Language Abstract)

Radiation energy balance at the top of atmosphere is crucial to the Earth climate system and is routinely examined in climate model validations. Here, we show that seemingly good agreements between model and observation can be due to compensating errors and propose the use of a kernel method for separately identifying component radiation biases due to different geophysical variables, which may afford a more stringent test of climate models.

Key Points

1. Climate models are subject to compensating radiation biases caused by cloud and non-cloud variables.
2. Many models have a cold temperature bias and a moist humidity bias in the troposphere.
3. Kernel diagnosis of component radiation biases affords a stricter test for climate models.

1. Introduction

Radiation energy balance at the top of the atmosphere (TOA) critically shapes the Earth climate. The global mean values of the longwave and shortwave radiation fluxes, as well as their distribution patterns are often used to validate the simulations of the global climate models (GCMs) (e.g., Kiehl et al. 1994; Su et al. 2010; Li et al. 2013; Dolinar et al. 2015; Loeb et al. 2020; Wild 2020). As illustrated by Fig. 1 (a) to (f) and also by others (e.g., Zhao et al. 2018; Golaz et al. 2019), the state-of-the-art GCMs show remarkable skills in reproducing observed climatological mean radiation fields, including the net radiation and its longwave and shortwave components.

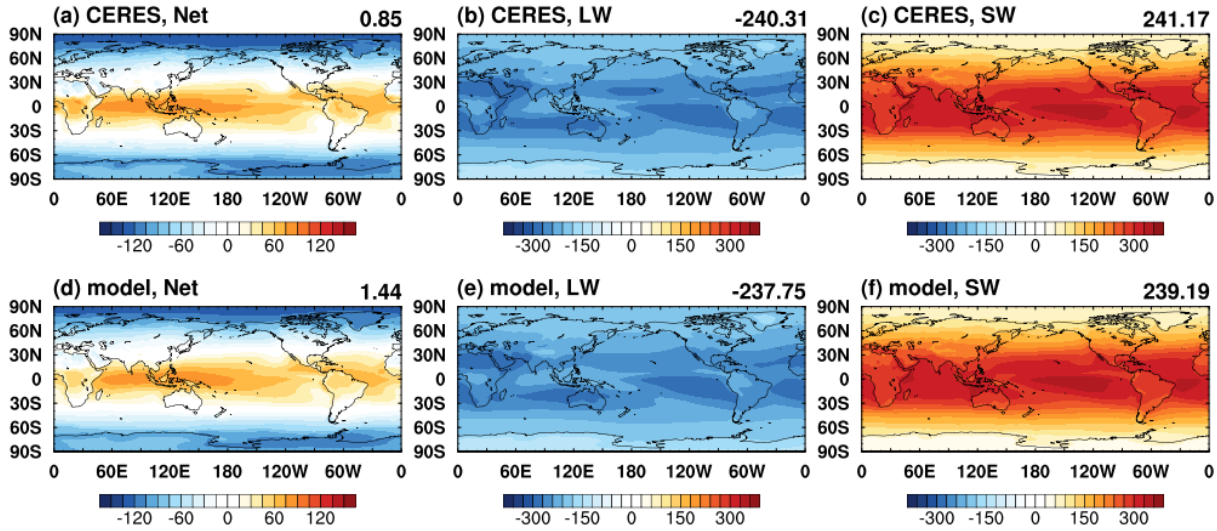

Figure 1. Climatological mean radiative fluxes in all-sky (units: W m^{-2}) from (a, b, c) the CERES satellite observation, and (d, e, f) multi-model mean of the AMIP simulations of GCMs. Global mean values are shown on the upper-right corner in each panel. AMIP: Atmospheric Modelling Intercomparison Project; GCM: Global Climate Model; CERES: Clouds and the Earth's Radiant Energy System.

However, the validation of GCMs with regard to overall radiation field is known to conceal possible compensating errors (Huang et al. 2007; Huang and Ramaswamy 2008; Huang, X. et al. 2008, 2013; Bani Shahabadi et al. 2016; Della Fera et al. 2022). For example, Huang et al. (2007) showed, by validating a GCM against spectrally resolved satellite radiance, that a seemingly good all-sky OLR field may result from compensating radiation errors due to the biases in the cloud fields and those in the non-cloud fields, such as the atmospheric temperature and humidity. On the other hand, comparisons of geophysical variables between GCM simulations and observations, such as the satellite retrieval products, verify the biases in the non-radiation fields. Some of these biases, such as those in the tropospheric humidity and temperature, appear to be persistent in a number of models (Gettelman et al. 2006, Jiang et al. 2015). These recognitions thus bear important questions: Is the agreement in the radiation fields between the latest GCMs and observations, as shown in Fig. 1, subject to compensating errors? And how much do different geophysical variables respectively contribute to the total radiation bias?

To answer the above questions, especially the latter one, it is important to have a comprehensive view of the error budget of the radiation fields and the ability to identify the biases that matter the most energetically. Among the potential causes of radiation errors, clouds are broadly conceived to be a major source of uncertainty in GCM simulations. This can and should be confirmed by quantifying the cloud-induced radiation bias and compare it to those caused by other geophysical variables. If, as revealed by previous studies (e.g., Huang et al. 2007), the cloud fields were tuned to compensate non-cloud biases in order for the model-simulated all-sky radiation to match the observation, the model would have cloud and non-cloud radiation biases of comparable magnitudes and opposite signs. On a relevant note, radiation biases are often cited to justify the need of treating certain processes in the GCMs. A recent example is the inclusion of the longwave scattering effect of clouds in the radiation codes (e.g., Chen et al. 2020). However, the impact of a proposed modification cannot be properly expected without a "big-picture" knowledge, i.e., what other, possibly more dominant, radiation biases exist in the models. These issues emphasize the need to separately quantify the individual radiation biases. This is important to verify that the radiation agreement in a model is achieved for the right reasons, or to identify which variable fields or physical processes are the most imperative to improve.

In this paper, we use a radiative kernel method to quantify the radiative biases caused by different geophysical variables, including surface and atmospheric temperature, humidity, surface albedo and clouds. The method and data are presented in Section 2. A systematic assessment of the radiative biases in the current GCMs is shown in Section 3.

2. Method

2.1 Observation and GCM data

To quantify the biases in the GCM-simulated radiation fields, we use the satellite observation of the Clouds and the Earth's Radiant Energy System (CERES, Wielicki et al., 1996) as the reference values of the TOA radiation fluxes. Specifically, its Energy Balanced and Filled (EBAF) dataset, version 4.2, with clear-sky radiation value consistently defined as in the GCMs (Loeb et al. 2018, 2020) is used. All the radiative fluxes are defined to be downward positive.

To quantify the GCM biases in the geophysical variables, we use the fifth generation European Centre for Medium-Range Weather Forecasts atmospheric reanalysis (ERA5) (Hersbach et al., 2020) as the reference values of such variables as surface and atmospheric temperature, water vapor, surface albedo.

The GCMs examined here are the models of the sixth phase of the Coupled Model Intercomparison Project (CMIP6, Eyring et al., 2016). Particularly, the Atmospheric Modelling Intercomparison Project (AMIP) simulations of the same period as the CERES data, years 2001-2014, are used here for analysis. A list of the models included in this analysis are summarized in the Supplementary Table S1.

2.2 Quantification of component biases: Kernel method

Radiative kernels, $\frac{\partial R}{\partial x}$, are pre-calculated radiative sensitivities to different geophysical variables, x, including surface temperature, atmospheric temperature and water vapor at different altitudes, and surface albedo. In this work, we use the radiative kernels computed by Huang & Huang (2023, under review) based on the ERA5 global reanalysis dataset. When multiplied by an anomaly of the geophysical variable, Δx, the product measures the radiation difference due to this anomaly:

$$\Delta R_x = \frac{\partial R}{\partial x}\Delta x \qquad (1)$$

Consider Δx to be the bias of the geophysical variable x with respect to a reference value, which we take from ERA5 reanalysis of the same period in this study; then the above equation measures radiative bias caused by x, which is a main objective here. The multi-model mean biases in the geophysical variables are shown in Supplementary Information (Fig. S1).

Radiative kernels have been widely used for radiative analyses, e.g., for quantifying climate feedbacks (e.g., Soden & Held 2006, Shell et al. 2008). A known limitation of Equation (1) is that it cannot be readily applied to cloud property variables whose effects on the radiation fields are strongly nonlinear. Hence, adopting the adjusted cloud radiative effect method used in feedback analysis (Shell et al. 2008), we measure the cloud-induced radiative bias essentially as a residual effect:

$$\Delta R_C = (\Delta R - \Delta R^0) - \sum_x (\Delta R_x - \Delta R_x^0) \qquad (2)$$

Here, ΔR and ΔR^0 are the all-sky and clear-sky total radiative biases in any of the TOA radiation fluxes: longwave (LW), shortwave (SW) or Net (LW+SW). ΔR_x and ΔR_x^0 are the all-sky and clear-sky component radiative biases caused by a non-cloud geophysical variable, as measured by Equation (1). Note the first term on the right-hand side of Equation (2) is the model bias in cloud radiative effect (CRE),

$$\Delta CRE = \Delta(R - R^0) \qquad (3)$$

which is often used to measure cloud-induced radiation bias but as discussed in the *Results* section is subject to errors.

As we use different datasets as the references of radiation fluxes (CERES) and geophysical variables (ERA5), it is worth examining their consistency. The Supplementary Fig. S2 shows the radiation biases of CMIP6 models against CERES and ERA5 are similar. Together with the radiation closure tests presented below, which verifies that the total bias ΔR can be explained by the sum of the component biases $\sum \Delta R_x$, this verifies the validity of using the geographical variables from ERA5 to diagnose the radiation biases against CERES.

3. Results

3.1 Global mean total radiation bias

According to the CERES data, the global annual mean all-sky longwave and shortwave radiation fluxes for the period of 2001-2014 are 240.31 and 241.17 W m^{-2}, respectively. As summarized in Table 1 and illustrated by Fig. 1, the CMIP6 models generally well reproduce these radiation fluxes, with multi-model mean biases in the global mean values being 2.57 and -1.97 W m^{-2} (in the order of 1%) and the root-mean-squares (RMS, which measure the magnitude of the biases regardless of their signs) being 3.89 and 4.20 W m^{-2}; see Supplementary Table S1 and S2 for the biases in the individual models.

		All-sky			Clear-sky		
		Longwave	Shortwave	Net	Longwave	Shortwave	Net
CERES observation		-240.31	241.17	0.85	-266.29	286.61	20.32
	Overall radiation biases (model minus observation)						
CMIP6 model bias	mean	2.57	-1.97	0.59	3.99	0.98	4.97
	RMS	3.89	4.20	2.32	4.68	2.54	6.35
	Kernel-diagnosed component radiation biases						
total bias	mean	1.58	-2.50	-0.92	3.00	0.45	3.46
	RMS	3.48	3.96	2.97	3.84	2.25	5.22
Surface (land) temperature	mean	-0.17	---	-0.17	-0.26	---	-0.26
	RMS	0.31		0.31	0.45		0.45
Atmospheric temperature	mean	1.78	---	1.78	1.62	---	1.62
	RMS	2.66		2.66	2.44		2.44
Water vapor	mean	1.31	0.19	1.50	1.64	0.09	1.73
	RMS	2.00	0.27	2.26	2.52	0.14	2.66
Surface albedo	mean	---	0.42	0.42	---	0.37	0.37
	RMS		1.74	1.74		2.20	2.20
Cloud	mean	-1.34	-3.11	-4.45	---	---	---
	RMS	2.88	5.04	5.24			
Residual	mean	0.98	0.53	1.51	0.98	0.53	1.51
	RMS	2.20	1.86	2.87	2.20	1.86	2.87

Table 1. The radiation biases in the CMIP6 models. Units: W m^{-2}. Summarized in this table are the multi-model mean and root-mean-square (RMS) of the biases in the global mean radiation fluxes of all the models examined (their respective biases are documented in Supplementary Tables S1 and S2).

Although the CMIP6 GCMs generally achieve excellent accuracy in their simulations of the all-sky global mean radiation budget, it is interesting to note that many of these models have larger clear-sky global mean biases than the all-sky ones. For the global mean TOA net radiation (the sum of longwave and shortwave fluxes) as an example, the RMS biases are 2.32 W m^{-2} in the all-sky and 6.35 W m^{-2} in the clear-sky. These results indicate that compensating errors caused by cloud and non-cloud variables noted in earlier studies (e.g., Huang et al. 2007) still exist in the current models. If a GCM has biases in non-cloud variables (as indicated by clear-sky radiation biases), when its cloud fields are tuned to match the observed all-sky radiation values,

it will have to produce cloud biases to offset non-cloud biases, to achieve a seeming agreement with the observations. This means that besides the cloud biases that are widely recognized and often emphasized, it is equally important to address the radiation biases due to non-cloud variables, to simulate a truly correct radiation budget in the GCMs.

Moreover, as illustrated by the standard deviation of the model biases in Table S3, the relative biases between the GCMs are of similar magnitudes to the multi-model mean and RMS biases. This aspect of the model bias is independent of the choice of truth reference (for which the CERES dataset is used in this study).

3.2 Component radiation bias

The diagnosis above signifies the importance of quantifying the radiation biases induced by different geophysical variables individually. Here, we use the kernel method described in Section 2.2 to measure the component radiation biases caused by each of these variables: surface temperature, atmospheric temperature, water vapor, surface albedo and cloud. It is worth noting that although the GCMs can generally well reproduce the global mean radiation budget compared to CERES, there exist regional biases of greater magnitudes, which as revealed below can be an order of magnitude larger than the global mean biases. It is thus important to examine the component radiation bias at both global and regional scales.

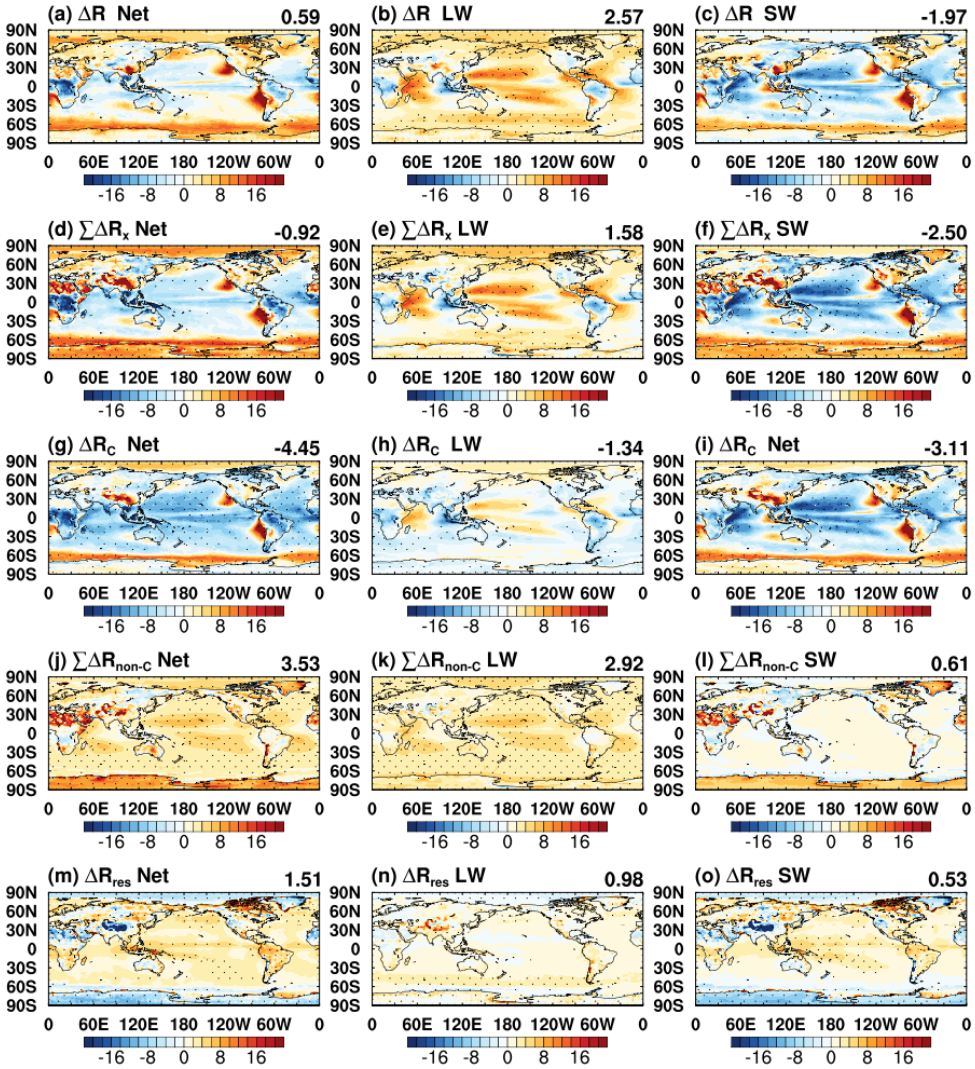

Figure 2. The multi-model mean total and component all-sky radiation biases in the CMIP6 models; units: W m^{-2}. Shown in the three columns are the Net, longwave and shortwave biases, respectively. Shown in the different rows are ΔR: the total bias, $\sum \Delta R_x$: the sum of all the component biases diagnosed from the kernel method, ΔR_C: the radiation bias due to cloud, ΔR_{non-C}: the radiation bias due to non-cloud variables, and ΔR_{res}: the unexplained bias residual. The dotted areas indicate where the multi-model mean bias is larger than the standard deviation.

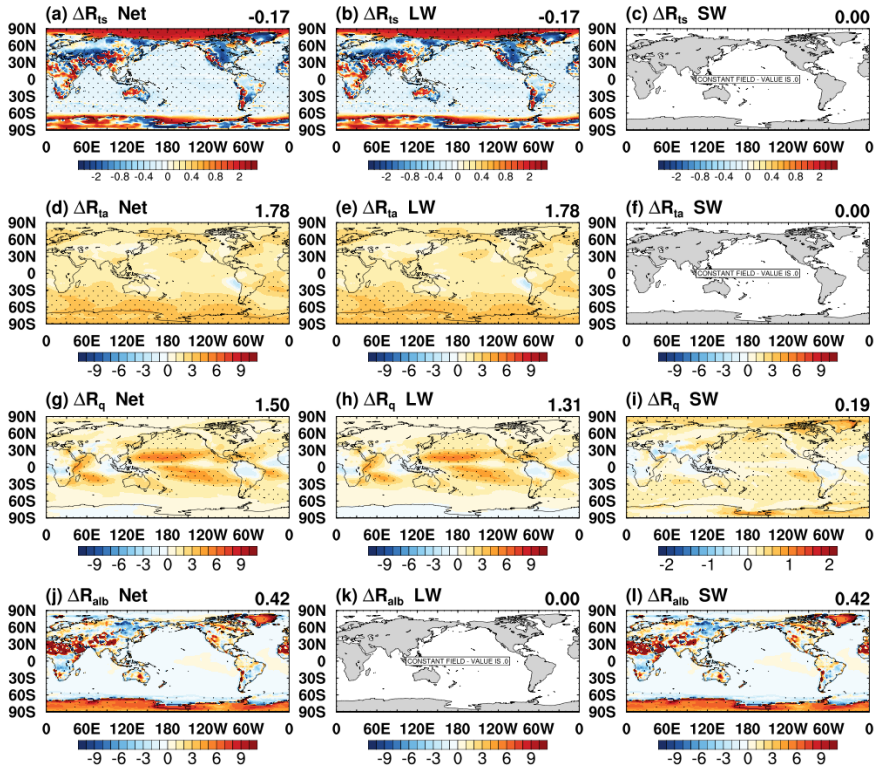

Figure 3. Like Figure 2, but for component radiation biases diagnosed by the kernel method. Shown in the different rows in order are the biases by surface temperature (ΔR_{ts}), air temperature (ΔR_{ta}), water vapor (ΔR_q), and surface albedo (ΔR_{alb}).

Fig. 2 and 3 show the global distributions of the total and component radiation biases averaged from all the models examined here; it complements the global mean bias values summarized in Table 1. In addition, interested readers can find the spatial correlation between the component and total radiation biases in the Supplementary Table S4 and S5, the distributions of the multi-model mean clear-sky biases in Figures S3 and S4, and the component radiation biases in each model in the Supplementary datafile.

The results in Fig. 2 affirm that kernel-diagnosed radiation biases ($\sum \Delta R_x$) can explain the majority of the total radiation biases (ΔR) in GCMs; their spatial correlations are 0.84, 0.69 and 0.70 for the longwave, shortwave and net radiation, respectively; the performance as measured by spatial correlation for each model is documented in Supplementary Table S4 and S5. The generally small residuals ($\Delta R_{res} = \Delta R - \sum \Delta R_x$) indicate that the kernel method achieves a good radiation closure in explaining the total ΔR, especially for the longwave radiation budget.

Cloud-induced radiation biases are well recognized to be a primary contributor to the total radiation biases. Table 1 and Fig. 2 (g-i) show that it has the largest global mean biases, as well as prominent regional biases, which explain most of the spatial variance of the total biases (see the spatial correlation coefficients in Supplementary Table S4, which is typically about 0.8). Using the RMS of bias values in every grid point, we find the all-sky spatial biases in the CMIP6 models are typically in the order of several W m^{-2}, although some models have larger values exceeding 10 W m^{-2} (see Supplementary Table S6), which are mainly contributed by the cloud

biases. The cloud biases are noticeably larger in the shortwave than in the longwave, as shown by the multi-model mean in Fig. 2, which shows local maxima exceeding 15 W m $^{-2}$ (the maximum biases in the individual models may exceed 50 W m $^{-2}$). We find strong, common biases in the stratocumulus regions in the eastern side of the ocean basins, e.g., adjacent to the coasts of California and Peru, where considerably less solar radiation is reflected by the modelled clouds compared to the CERES observation. In the rest of the tropical ocean, modelled clouds tend to be too reflective. These shortwave biases are offset to some extent by the longwave cloud biases, due to the compensating nature of cloud radiative effects.

We also find significant biases caused by the non-cloud variables. Some of them have global mean magnitudes comparable to the cloud biases (Table 1). In particular, we find that many models have a cold bias in the air temperature and moist bias in the water vapor concentration in the troposphere (see Fig S1), both of which lead to an underestimation of the outgoing longwave radiation - a positive bias in terms of TOA radiation budget (downward positive). As marked by the shaded areas in Fig. 3 (d) and (g), the water vapor bias and air temperature bias lead to radiation biases in many models in Tropical Pacific and Southern Oceans, respectively. Interestingly, these positive non-cloud biases tend to be compensated by cloud biases of an opposite sign, which in some models results in a seemingly good all-sky radiation budget (see Tables 1 and S1) as noted above.

It is worth noting that cloud bias is often measured by the cloud radiative effect (ΔCRE, as given in Equation (3)). Because this quantity depends on the clear-sky radiation field, this potentially aliases model errors in clear-sky radiation fields caused by the non-cloud variables as cloud bias. In comparison, the cloud bias ΔR_C measured by Equation (2) explicitly deducts the contributions from non-cloud variables to the total radiation bias (ΔR) and thus is less subject to such aliasing errors. Comparing ΔR_C and ΔCRE in the CMIP6 GCMs, we find that except in several models (see Supplementary Table S1), the two measures agree to within 10% in terms of global mean cloud biases. However, as illustrated by Supplementary Fig. S5, in some models and especially in regions where non-cloud biases prevail such as in the Arctic, the use of ΔCRE can strongly bias the measure of cloud radiative bias.

4. Discussions and Conclusions

In this paper, we propose and demonstrate the use of radiative sensitivity kernels for diagnosing the radiation biases in the GCMs. Using this method, we assess the TOA radiation fluxes simulated in the AMIP runs of the CMIP6 climate models against the CERES satellite observations and quantify how the total model biases in the net, longwave and shortwave radiation fields result from the biases in their geophysical variables, including surface temperature and albedo, atmospheric temperature and water vapor concentration, and cloud.

In terms of global mean radiation fluxes, the CMIP6 models can well reproduce the CERES-observed all-sky values. However, we find many of the models have larger biases in the clear-sky global mean radiation budget, with the biases in the net radiation fluxes typically amounting to several W m^{-2} and being several times of their all-sky values (Tables 1 and S1). This signifies the existence of compensating errors in their simulated radiation fields.

Specifically, cloud biases, possibly due to model tuning, compensate the radiation biases caused by non-cloud variables.

Cloud-induced radiation bias makes a primary contribution to the total radiation bias. This is especially the case for the shortwave radiation field, where significant biases are found in the tropical regions, signifying errors in cloudiness and thus reflected solar radiation.

Concerning the non-cloud biases, we find that many models have a cold bias in the air temperature and a moist bias in the tropospheric humidity compared to the ERA5 reanalysis. These biases each lead to a global mean radiation bias in the magnitude of several W m^{-2} (Tables 1 and S1), and persistent regional biases especially in the Tropical and middle-latitude oceans (Fig. 3). This means that the GCMs cannot achieve a good (better than several W m^{-2}) radiation closure compared to the observation benchmarks without addressing these non-cloud biases.

The kernel method used here aims to obtain a first-order quantification of the component radiation biases. Given its linear approximation nature (Equation (1)), it is inevitable to leave residuals in the model error budget. Moreover, the uncertainty of greenhouse gas and aerosols prescribed in the models may also contribution to the residuals. Nevertheless, the explained bias ($\sum \Delta R_x$) is generally strongly spatially correlated with the total flux biases (ΔR) (see Table S4 and S5), indicating the method can explain the majority of model biases. Another notable strength of it is that it avoids the aliasing issue in quantifying the cloud radiative bias. The significant component biases, namely the cloud, air temperature and tropospheric humidity biases, disclosed by this method warrant further investigations.

Acknowledgements

We thank Yuwei Wang and Jing Feng for their helpful comments. We acknowledge the grants from the Natural Sciences and Engineering Research Council of Canada (RGPIN-2019-04511) and the Fonds de Recherché Nature et Technologies of Quebec (2021-PR-283823) that supported this research.

Data Availability Statement

The ERA5 datasets can be accessed through the ECMWF website (C3S, 2017). The ERA5-based radiative kernels can be downloaded at H. Huang (2023a). The kernel-diagnosed total and component radiation biases in all the CMIP6 models examined here can be obtained from: H. Huang (2023b).

References

Bani Shahabadi, M., Huang, Y., Garand, L., Heilliette, S., and Yang, P. (2016), Validation of a weather forecast model at radiance level against satellite observations allowing quantification of temperature, humidity, and cloud-related biases, *J. Adv. Model. Earth Syst.*, 8, 1453– 1467, doi:10.1002/2016MS000751.

Chen, Y. H., Huang, X., Yang, P., Kuo, C. P., & Chen, X. (2020). Seasonal dependent impact of ice cloud longwave scattering on the polar climate. *Geophysical Research Letters*, 47(23), e2020GL090534.

Copernicus Climate Change Service (C3S) (2017). ERA5 [Dataset]: Fifth generation of ECMWF atmospheric reanalyses of the global climate . Copernicus Climate Change Service Climate Data Store (CDS), date of access. https://cds.climate.copernicus.eu/cdsapp#!/home

Della Fera, S., Fabiano, F., Raspollini, P., Ridolfi, M., Cortesi, U., Barbara, F., and von Hardenberg, J. (2022) On the use of IASI spectrally resolved radiances to test the EC-Earth climate model (v3.3.3) in clear-sky conditions, EGUsphere [preprint], https://doi.org/10.5194/egusphere-2022-479.

Dolinar, E.K., Dong, X., Xi, B. et al. Evaluation of CMIP5 simulated clouds and TOA radiation budgets using NASA satellite observations. Clim Dyn 44, 2229–2247 (2015). https://doi.org/10.1007/s00382-014-2158-9

Eyring, V., Bony, S., Meehl, G. A., Senior, C. A., Stevens, B., Stouffer, R. J., & Taylor, K. E. (2016). Overview of the Coupled Model Intercomparison Project Phase 6 (CMIP6) experimental design and organization. *Geoscientific Model Development*, 9(5), 1937-1958.

Golaz, J. C., Caldwell, P. M., Van Roekel, L. P., Petersen, M. R., Tang, Q., Wolfe, J. D., ... & Zhu, Q. (2019). The DOE E3SM coupled model version 1: Overview and evaluation at standard resolution. *Journal of Advances in Modeling Earth Systems*, 11(7), 2089-2129. https://doi.org/10.1029/2018MS001603

Gettelman, A., Collins, W. D., Fetzer, E. J., Eldering, A., Irion, F. W., Duffy, P. B., & Bala, G. (2006). Climatology of Upper-Tropospheric Relative Humidity from the Atmospheric Infrared Sounder and Implications for Climate, *Journal of Climate*, *19*(23), 6104-6121. https://journals.ametsoc.org/view/journals/clim/19/23/jcli3956.1.xml

Hersbach, H., Bell, B., Berrisford, P., Hirahara, S., Horányi, A., Muñoz-Sabater, J., Schepers, D. (2020). The ERA5 global reanalysis. Quarterly Journal of the Royal Meteorological Society, 146(730), 1999-2049.

Huang, Han (2023a), “Data for ERA5 radiative kernels”, Mendeley Data, V2, doi: 10.17632/vmg3s67568.2

Huang, Han (2023b), “Data for "diagnosing the radiation biases in the global climate models using relative kernels"”, Mendeley Data, V2, doi: 10.17632/6j5999szj6.2

Huang, H., & Huang, Y. (2023). Radiative sensitivity quantified by a new set of radiation flux kernels based on the ERA5 reanalysis, *Earth System Science Data*, (under review).

Huang, X., Yang, W., Loeb, N. G., and Ramaswamy, V. (2008), Spectrally resolved fluxes derived from collocated AIRS and CERES measurements and their application in model evaluation: Clear sky over the tropical oceans, *J. Geophys. Res.*, 113, D09110, doi:10.1029/2007JD009219.

Huang, X., Cole, J. N. S., He, F., Potter, G. L., Oreopoulos, L., Lee, D., Suarez, M., & Loeb, N. G. (2013). Longwave Band-By-Band Cloud Radiative Effect and Its Application in GCM Evaluation, *Journal of Climate*, *26*(2), 450-467. Retrieved Sep 13, 2022, from https://journals.ametsoc.org/view/journals/clim/26/2/jcli-d-12-00112.1.xml

Huang, Y., Ramaswamy, V., Huang, X., Fu, Q., and Bardeen, C. (2007), A strict test in climate modeling with spectrally resolved radiances: GCM simulation versus AIRS observations, *Geophys. Res. Lett.*, 34, L24707, doi:10.1029/2007GL031409.

Huang, Y., & Ramaswamy, V. (2008). Observed and simulated seasonal co-variations of outgoing longwave radiation spectrum and surface temperature. *Geophys. Res. Lett.*, 35(17).

Jiang, J. H., Su, H., Zhai, C., Wu, L., Minschwaner, K., Molod, A. M., and Tompkins, A. M. (2015), An assessment of upper troposphere and lower stratosphere water vapor in MERRA, MERRA2, and ECMWF reanalyses using Aura MLS observations, *J. Geophys. Res. Atmos.*, 120, 11,468– 11,485, doi:10.1002/2015JD023752.

Kato, S., Rose, F. G., Rutan, D. A., Thorsen, T. J., Loeb, N. G., Doelling, D. R., Huang, X., Smith, W. L., Su, W., & Ham, S. (2018). Surface Irradiances of Edition 4.0 Clouds and the Earth’s Radiant Energy System (CERES) Energy Balanced and Filled (EBAF) Data Product, Journal of Climate, 31(11), 4501-4527.

Kiehl, J. T., Hack, J. J., and Briegleb, B. P. (1994), The simulated Earth radiation budget of the National Center for Atmospheric Research community climate model CCM2 and comparisons with the Earth Radiation Budget Experiment (ERBE), J. Geophys. Res., 99(D10), 20815–20827, doi:10.1029/94JD00941.

Li, J.-L. F., Waliser, D. E., Stephens, G., Lee, S., L'Ecuyer, T., Kato, S., Loeb, N., and Ma, H.-Y. (2013), Characterizing and understanding radiation budget biases in CMIP3/CMIP5 GCMs, contemporary GCM, and reanalysis, J. Geophys. Res. Atmos., 118, 8166– 8184, doi:10.1002/jgrd.50378.

Loeb, N. G., Doelling, D. R., Wang, H., Su, W., Nguyen, C., Corbett, J. G., Liang, L., Mitrescu, C., Rose, F. G., & Kato, S. (2018). Clouds and the Earth’s Radiant Energy System (CERES)

Energy Balanced and Filled (EBAF) Top-of-Atmosphere (TOA) Edition-4.0 Data Product, Journal of Climate, 31(2), 895-918.

Loeb, N. G., Rose, F. G., Kato, S., Rutan, D. A., Su, W., Wang, H., Doelling, D. R., Smith, W. L., & Gettelman, A. (2020). Toward a Consistent Definition between Satellite and Model Clear-Sky Radiative Fluxes, *Journal of Climate*, *33*(1), 61-75.

Shell, K. M., Kiehl, J. T., & Shields, C. A. (2008). Using the radiative kernel technique to calculate climate feedbacks in NCAR's Community Atmospheric Model. *Journal of Climate*, 21(10), 2269-2282.

Soden, B. J., & Held, I. M. (2006). An assessment of climate feedbacks in coupled ocean–atmosphere models. *Journal of climate*, 19(14), 3354-3360.

Su, W., Bodas-Salcedo, A., Xu, K.-M., and Charlock, T. P. (2010), Comparison of the tropical radiative flux and cloud radiative effect profiles in a climate model with Clouds and the Earth's Radiant Energy System (CERES) data, J. Geophys. Res., 115, D01105, doi:10.1029/2009JD012490.

Wielicki, B. A., B. R. Barkstrom, E. F. Harrison, R. B. Lee III, G. L. Smith, and J. E. J. B. o. t. A. M. S. Cooper (1996), Clouds and the Earth's Radiant Energy System (CERES): An earth observing system experiment, B Am Meteorol Soc, 77(5), 853-868.

Wild, M. (2020). The global energy balance as represented in CMIP6 climate models. *Clim Dyn* **55**, 553–577. https://doi.org/10.1007/s00382-020-05282-7

Zhao, M., Golaz, J.-C., Held, I. M., Guo, H., Balaji, V., Benson, R., et al. (2018). The GFDL global atmosphere and land model AM4.0/LM4.0: 1. Simulation characteristics with prescribed SSTs. *Journal of Advances in Modeling Earth Systems*, 10, 691– 734. https://doi.org/10.1002/2017MS001208

Zhang, M. H., Lin, W. Y., and Kiehl, J. T. (1998), Bias of atmospheric shortwave absorption in the NCAR Community Climate Models 2 and 3: Comparison with monthly ERBE/GEBA measurements, J. Geophys. Res., 103(D8), 8919– 8925, doi:10.1029/98JD00343.

Supplementary information for

Diagnosing the radiation biases in global climate models using radiative kernels

Han Huang, Yi Huang

Department of Atmospheric and Oceanic Sciences, McGill University, Montreal, Canada

Corresponding Authors:

Yi Huang, yi.huang@mcgill.ca (ORCID: 0000-0002-5065-4198)

Contents of this file

Table S1-S6, as shown in the spreadsheet file "dR_globalmean_eachModel.xlsx".

Figure S1-S5

Data file: dR_globalmap_eachModel.nc

Introductions

Tables S1 and S2 show the global mean values of the total and component radiation biases in every CMIP6 GCM examined in this work. The models shown here do not include all the GCMs submitted to CMIP6, as only one model from each modelling center is (arbitrarily) selected.

Table S3 shows the standard deviation of the biases in the global mean radiation fluxes of all the models.

Tables S4 and S5 show the spatial correlation between the global distributions of the total and component radiation biases in every CMIP6 GCM.

Table S6 shows the spatial root-mean-square-error in all the latitude-longitude grid points across the globe in each model.

Figure S1 shows the biases in GCM-simulated climate variables compared to ERA5.

Figure S2 compares the model radiation biases relative to CERES and those relative to ERA5.

Figures S3 and S4 show the multi-model mean model biases in the clear-sky.

Figure S5 compares the cloud radiation biases measured by the kernel and CRE methods.

Data file "dR_globalmap_eachModel.nc" records the global distributions of radiation biases in every model.

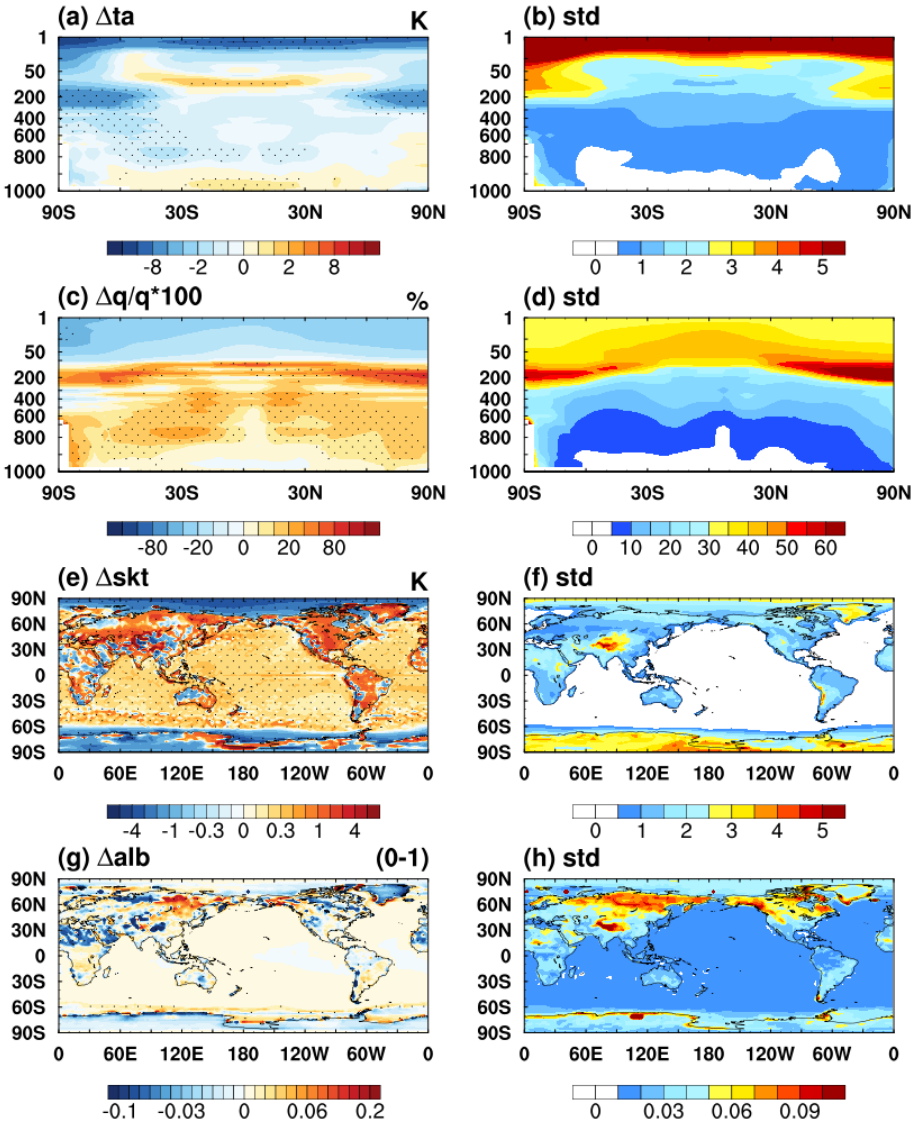

Figure S1. Multi-model mean and standard deviation (std) of the biases in modelled atmospheric variables compared to ERA5. (a, b) air temperature, units: K, (c, d) water vapor in fraction, units: %, (e, f) skin temperature, units: K, and (g, h) surface albedo. The stippled area in each panel signifies persistent biases, where the magnitude of the multi-model mean exceeds the standard deviation.

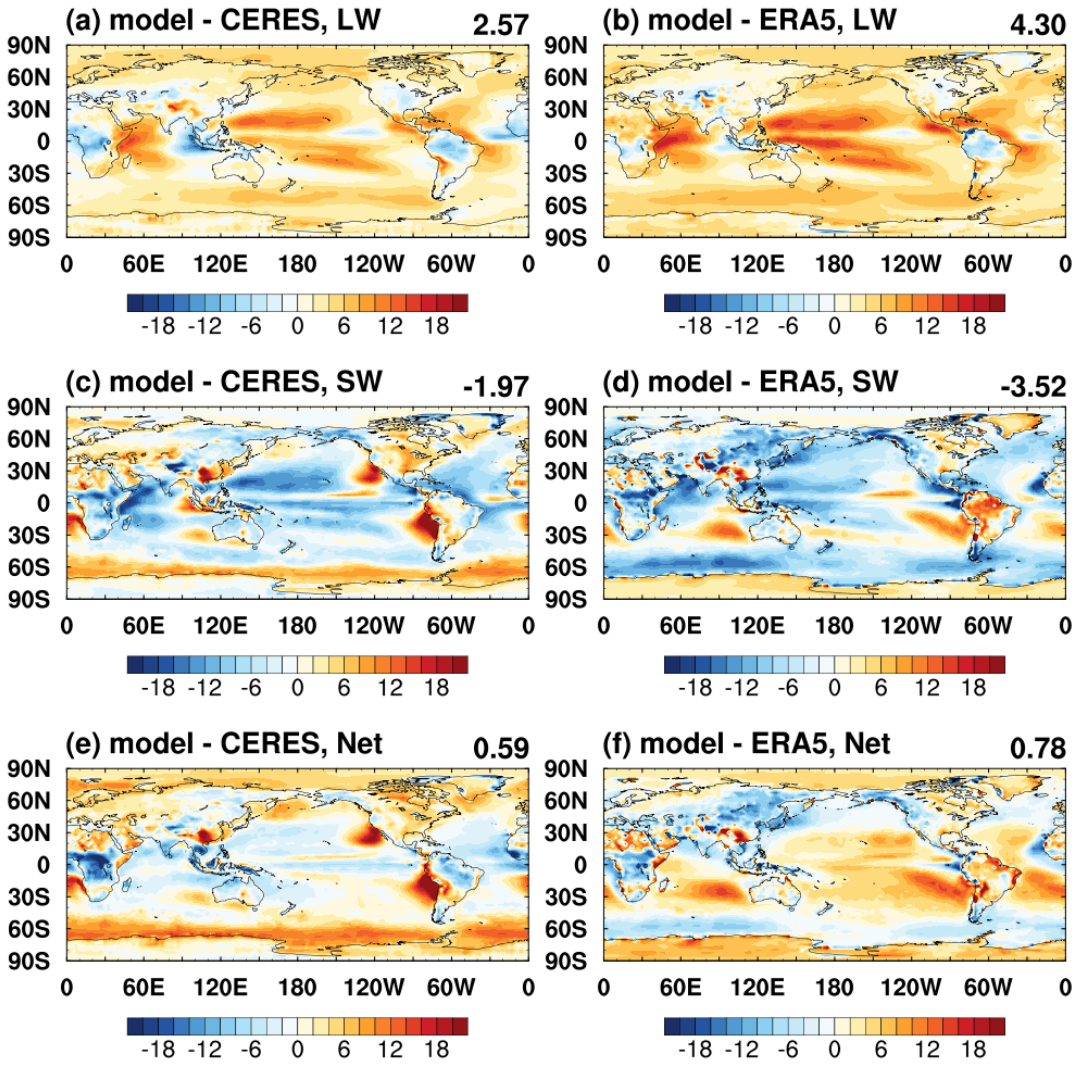

Figure S2. Multi-model mean all-sky radiation biases of the CMIP6 models compared to (a, c, e) CERES, and (b, d, f) ERA5; units: W m^{-2}. The number on the top right corner in each panel is the global mean value. The area-weighted spatial correlation between the biases relative to the two different references are: 0.80, 0.51 and 0.34 for the longwave, shortwave and net, respectively, showing their consistency.

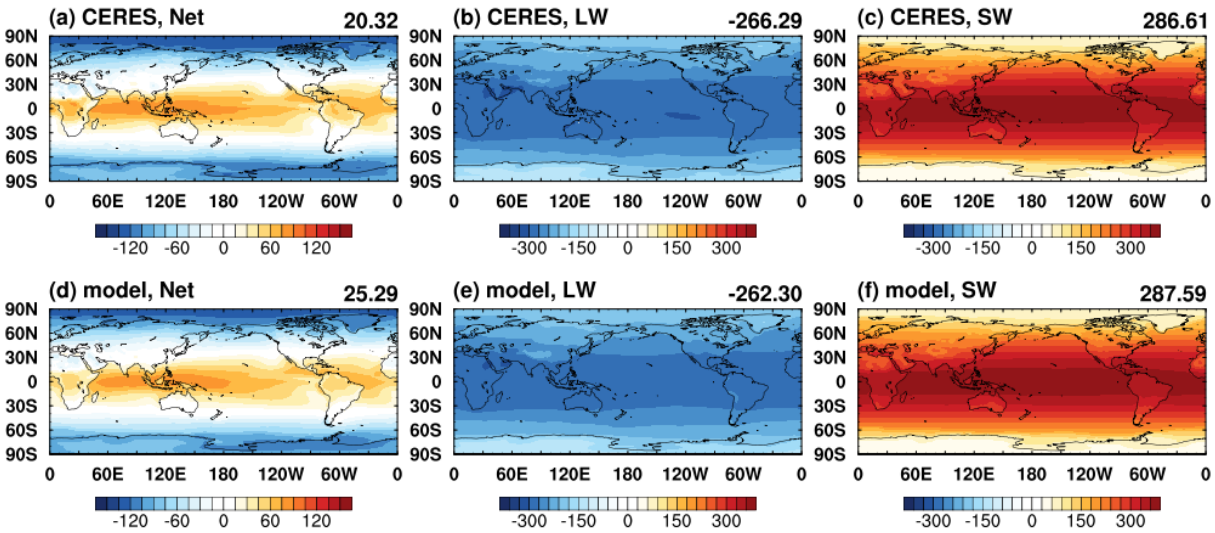

Figure S3. Like Fig. 1, but for the radiative fluxes in clear-sky (units: W m^{-2}) from (a, b, c) the CERES satellite observation, and (d, e, f) multi-model mean of the CMIP6 GCMs.

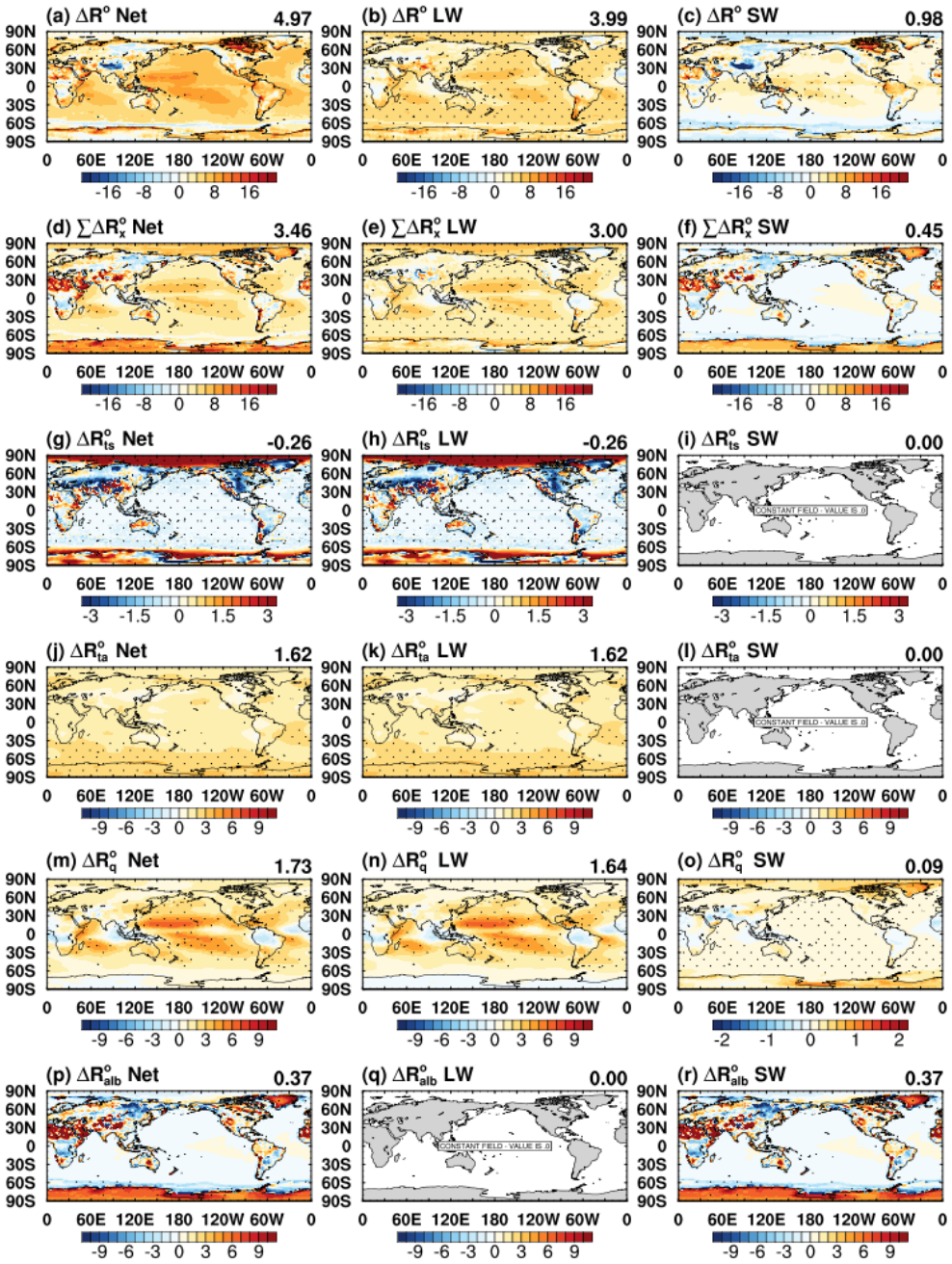

Figure S4. Similar to Fig. 3, but for the model radiation biases in the clear-sky.

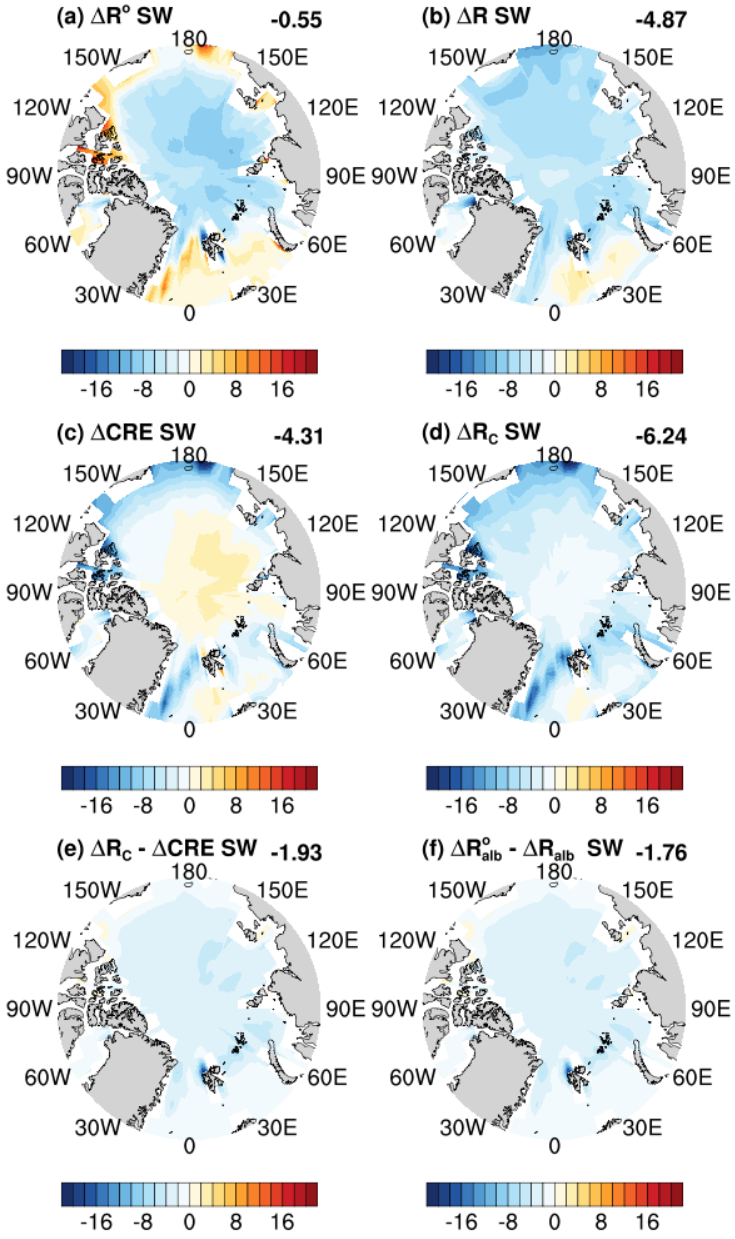

Figure S5. Comparison of cloud radiative biases measured by different methods. Shown here as an example are the radiation biases quantified for one GCM, the MPI-ESM1-2-LR model; units: W m^{-2}. (a) Clear-sky and (b) all-sky total radiation biases, and (c) their difference, i.e., cloud radiative bias measured by cloud radiative effect ΔCRE according to Equation (3). (d) Cloud radiative bias measured by the kernel method ΔR_C according to Equation (2). Their difference as shown in (e), is due to the aliasing effect caused by the surface albedo bias as shown in (f). Examining the CMIP6 GCMs one by one, we find this aliasing bias exist in a majority of the models (see the NetCDF data file documenting the component biases in the individual models).

Table S1. All-sky total (dR) and component (dRx) global mean radiation biases in each model; units: W m-2.

		LW									SW									Net								
Model #	Model name	dR	sumdR	dRts	dRta	dRq	dRalb	dRc	dCRE	res	dR	sumdR	dRts	dRta	dRq	dRalb	dRc	dCRE	res	dR	sumdR	dRts	dRta	dRq	dRalb	dRc	dCRE	res
1	ACCESS-CM2	-1.34	-1.99	-0.38	0.70	1.03	0.00	-3.33	-3.31	0.65	0.90	1.63	0.00	0.00	0.08	0.68	0.87	0.97	-0.73	-0.43	-0.35	-0.38	0.70	1.11	0.68	-2.46	-2.35	-0.08
2	BCC-ESM1	8.01	9.33	-0.27	2.36	3.68	0.00	3.56	3.12	-1.32	-7.73	-5.01	0.00	0.00	0.43	5.17	-10.61	-11.64	-2.72	0.28	4.32	-0.27	2.36	4.11	5.17	-7.06	-8.52	-4.04
3	CanESM5	0.84	0.04	0.23	0.24	0.55	0.00	-0.97	-1.02	0.80	1.31	-0.90	0.00	0.00	0.00	-0.82	-0.08	0.28	2.21	2.15	-0.85	0.23	0.24	0.55	-0.82	-1.05	-0.73	3.01
4	CAS-ESM2-0	4.19	3.42	-0.02	4.59	2.96	0.00	-4.10	-4.48	0.77	3.72	0.25	0.00	0.00	0.34	2.23	-2.32	-2.61	3.47	7.91	3.67	-0.02	4.59	3.30	2.23	-6.42	-7.10	4.23
5	CESM2	2.17	1.01	-0.16	2.71	0.80	0.00	-2.34	-2.30	1.16	0.52	-1.30	0.00	0.00	0.18	0.76	-2.24	-2.23	1.81	2.69	-0.29	-0.16	2.71	0.98	0.76	-4.58	-4.52	2.97
6	CIESM	1.88	1.60	-0.14	2.28	3.62	0.00	-4.15	-5.21	0.28	0.40	1.77	0.00	0.00	0.54	1.01	0.22	0.26	-1.36	2.28	3.37	-0.14	2.28	4.16	1.01	-3.93	-4.95	-1.09
7	CMCC-CM2-SR5	1.16	0.53	-0.05	3.03	2.00	0.00	-4.45	-4.81	0.63	3.25	1.15	0.00	0.00	0.34	1.58	-0.77	-1.00	2.10	4.41	1.68	-0.05	3.03	2.34	1.58	-5.22	-5.81	2.73
8	CNRM-ESM2-1	1.67	0.50	-0.17	5.82	-0.57	0.00	-4.59	-3.68	1.17	-1.47	-2.22	0.00	0.00	0.00	0.59	-2.82	-2.82	0.75	0.20	-1.72	-0.17	5.82	-0.57	0.59	-7.40	-6.50	1.93
9	E3SM-1-0	1.05	0.38	-0.12	1.15	0.88	0.00	-1.52	-1.50	0.67	-1.57	-3.10	0.00	0.00	0.27	0.65	-4.02	-4.04	1.53	-0.51	-2.72	-0.12	1.15	1.15	0.65	-5.54	-5.54	2.20
10	EC-Earth3	0.47	-0.88	-0.21	-0.07	-0.58	0.00	-0.01	0.36	1.35	-1.59	-1.37	0.00	0.00	-0.09	-0.47	-0.82	-0.58	-0.21	-1.11	-2.25	-0.21	-0.07	-0.67	-0.47	-0.83	-0.22	1.14
11	FGOALS-g3	5.11	6.38	0.16	5.99	-0.22	0.00	0.44	0.85	-1.27	-4.31	-1.81	0.00	0.00	-0.01	0.44	-2.23	-2.16	-2.51	0.80	4.57	0.16	5.99	-0.23	0.44	-1.79	-1.31	-3.78
12	GFDL-CM4	1.18	-2.82	-0.03	0.11	-0.24	0.00	-2.66	-2.48	3.99	-1.47	-3.59	0.00	0.00	0.00	-0.39	-3.20	-2.88	2.12	-0.29	-6.40	-0.03	0.11	-0.24	-0.39	-5.86	-5.35	6.11
13	GISS-E2-2-G	6.78	1.41	0.17	4.91	-1.19	0.00	-2.47	-1.55	5.37	-7.75	-5.12	0.00	0.00	-0.17	1.04	-5.99	-6.16	-2.63	-0.97	-3.71	0.17	4.91	-1.36	1.04	-8.46	-7.71	2.74
14	HadGEM3-GC31-	-0.77	-2.02	-0.32	0.67	1.08	0.00	-3.44	-3.44	1.24	0.22	0.36	0.00	0.00	0.08	-0.56	0.84	1.34	-0.14	-0.55	-1.66	-0.32	0.67	1.16	-0.56	-2.60	-2.10	1.10
15	IITM-ESM	5.08	3.46	-0.75	0.75	-1.15	0.00	4.60	5.44	1.61	-8.98	-7.73	0.00	0.00	0.03	2.00	-9.77	-9.96	-1.25	-3.90	-4.27	-0.75	0.75	-1.12	2.00	-5.16	-4.53	0.37
16	INM-CM5-0	-1.46	-0.15	-0.09	-0.78	2.50	0.00	-1.79	-2.92	-1.31	0.35	-1.24	0.00	0.00	0.31	-4.02	2.48	4.01	1.59	-1.11	-1.39	-0.09	-0.78	2.81	-4.02	0.69	1.09	0.28
17	IPSL-CM6A-LR	2.34	1.95	0.06	2.88	0.12	0.00	-1.12	-1.12	0.39	-0.92	-2.64	0.00	0.00	0.15	0.24	-3.03	-2.92	1.72	1.42	-0.69	0.06	2.88	0.27	0.24	-4.15	-4.04	2.11
18	MIROC-ES2L	10.48	4.48	-0.87	2.11	2.24	0.00	0.99	1.37	6.00	-10.34	-10.23	0.00	0.00	0.36	2.11	-12.70	-12.82	-0.11	0.14	-5.75	-0.87	2.11	2.60	2.11	-11.71	-11.45	5.89
19	MPI-ESM1-2-LR	1.64	0.76	-0.37	-0.45	2.58	0.00	-1.01	-1.52	0.89	-2.43	-2.04	0.00	0.00	0.34	0.01	-2.40	-2.09	-0.38	-0.78	-1.29	-0.37	-0.45	2.93	0.01	-3.41	-3.61	0.50
20	MRI-ESM2-0	1.20	-0.28	-0.22	-0.31	1.90	0.00	-1.65	-1.92	1.48	0.15	-2.13	0.00	0.00	0.19	-2.58	0.26	1.35	2.29	1.35	-2.41	-0.22	-0.31	2.09	-2.58	-1.39	-0.57	3.76
21	NESM3	3.96	3.39	-0.35	-1.10	4.12	0.00	0.73	-0.38	0.57	-3.42	-2.67	0.00	0.00	0.54	-0.07	-3.14	-2.71	-0.75	0.54	0.72	-0.35	-1.10	4.66	-0.07	-2.41	-3.09	-0.18
22	NorCPM1	5.08	8.63	0.08	2.35	2.46	0.00	3.74	3.36	-3.54	-6.52	-9.38	0.00	0.00	0.29	0.77	-10.44	-10.39	2.86	-1.44	-0.75	0.08	2.35	2.75	0.77	-6.70	-7.03	-0.69
23	SAM0-UNICON	1.50	1.00	0.13	2.01	1.78	0.00	-2.91	-3.27	0.50	0.10	-2.44	0.00	0.00	0.29	0.63	-3.36	-3.28	2.54	1.60	-1.44	0.13	2.01	2.07	0.63	-6.28	-6.55	3.04
24	UKESM1-0-LL	-0.63	-2.17	-0.38	0.70	1.14	0.00	-3.63	-3.66	1.55	0.18	-0.25	0.00	0.00	0.08	-0.89	0.57	1.16	0.43	-0.45	-2.42	-0.38	0.70	1.21	-0.89	-3.06	-2.50	1.97
	multi-model mear	2.57	1.58	-0.17	1.78	1.31	0.00	-1.34	-1.42	0.98	-1.97	-2.50	0.00	0.00	0.19	0.42	-3.11	-2.96	0.53	0.59	-0.92	-0.17	1.78	1.50	0.42	-4.45	-4.37	1.51

Table S2. Clear-sky total (dR) and component (dRx) global mean radiation biases in each model; units: W m-2.

		LW							SW							Net					
Model #	Model name	dR	sum(dRx)	dRts	dRta	dRq	dRalb	res	dR	sum(dRx)	dRts	dRta	dRq	dRalb	res	dR	sum(dRx)	dRts	dRta	dRq	dRalb	res
1	ACCESS-CM2	1.98	1.33	-0.56	0.61	1.28	0.00	0.65	-0.06	0.66	0.00	0.00	-0.02	0.69	-0.73	1.91	1.99	-0.56	0.61	1.26	0.69	-0.08
2	BCC-ESM1	4.89	6.21	-0.41	2.10	4.53	0.00	-1.32	3.90	6.63	0.00	0.00	0.21	6.41	-2.72	8.80	12.84	-0.41	2.10	4.74	6.41	-4.04
3	CanESM5	1.86	1.06	0.25	0.24	0.56	0.00	0.80	1.03	-1.18	0.00	0.00	-0.02	-1.16	2.21	2.89	-0.12	0.25	0.24	0.54	-1.16	3.01
4	CAS-ESM2-0	8.67	7.90	0.04	4.27	3.59	0.00	0.77	6.33	2.87	0.00	0.00	0.17	2.69	3.47	15.00	10.77	0.04	4.27	3.76	2.69	4.23
5	CESM2	4.47	3.30	-0.29	2.50	1.09	0.00	1.16	2.74	0.93	0.00	0.00	0.09	0.85	1.81	7.21	4.24	-0.29	2.50	1.18	0.85	2.97
6	CIESM	7.09	6.82	-0.13	2.27	4.68	0.00	0.28	0.14	1.50	0.00	0.00	0.29	1.21	-1.36	7.23	8.32	-0.13	2.27	4.96	1.21	-1.09
7	CMCC-CM2-SR5	5.97	5.34	-0.03	2.76	2.61	0.00	0.63	4.25	2.15	0.00	0.00	0.20	1.96	2.10	10.22	7.49	-0.03	2.76	2.81	1.96	2.73
8	CNRM-ESM2-1	5.35	4.18	-0.30	5.18	-0.71	0.00	1.17	1.35	0.60	0.00	0.00	-0.01	0.61	0.75	6.70	4.78	-0.30	5.18	-0.72	0.61	1.93
9	E3SM-1-0	2.55	1.88	-0.32	0.99	1.20	0.00	0.67	2.47	0.94	0.00	0.00	0.18	0.76	1.53	5.02	2.82	-0.32	0.99	1.38	0.76	2.20
10	EC-Earth3	0.12	-1.23	-0.42	-0.16	-0.65	0.00	1.35	-1.01	-0.80	0.00	0.00	-0.10	-0.70	-0.21	-0.89	-2.03	-0.42	-0.16	-0.75	-0.70	1.14
11	FGOALS-g3	4.26	5.53	0.27	5.68	-0.43	0.00	-1.27	-2.15	0.36	0.00	0.00	-0.04	0.39	-2.51	2.11	5.88	0.27	5.68	-0.46	0.39	-3.78
12	GFDL-CM4	3.65	-0.34	0.01	0.00	-0.35	0.00	3.99	1.41	-0.71	0.00	0.00	-0.01	-0.70	2.12	5.06	-1.05	0.01	0.00	-0.36	-0.70	6.11
13	GISS-E2-2-G	8.33	2.96	0.11	4.52	-1.67	0.00	5.37	-1.59	1.04	0.00	0.00	-0.08	1.13	-2.63	6.74	4.00	0.11	4.52	-1.75	1.13	2.74
14	HadGEM3-GC31-LL	2.67	1.43	-0.49	0.59	1.33	0.00	1.24	-1.12	-0.98	0.00	0.00	-0.02	-0.96	-0.14	1.55	0.45	-0.49	0.59	1.31	-0.96	1.10
15	IITM-ESM	-0.36	-1.97	-0.99	0.53	-1.52	0.00	1.61	0.98	2.23	0.00	0.00	0.03	2.19	-1.25	0.62	0.25	-0.99	0.53	-1.48	2.19	0.37
16	INM-CM5-0	1.46	2.77	-0.07	-0.39	3.22	0.00	-1.31	-3.66	-5.25	0.00	0.00	0.14	-5.39	1.59	-2.20	-2.48	-0.07	-0.39	3.36	-5.39	0.28
17	IPSL-CM6A-LR	3.46	3.07	0.05	2.75	0.27	0.00	0.39	2.00	0.28	0.00	0.00	0.10	0.19	1.72	5.46	3.35	0.05	2.75	0.37	0.19	2.11
18	MIROC-ES2L	9.11	3.11	-1.24	1.72	2.63	0.00	6.00	2.48	2.59	0.00	0.00	0.21	2.37	-0.11	11.59	5.70	-1.24	1.72	2.85	2.37	5.89
19	MPI-ESM1-2-LR	3.16	2.27	-0.55	-0.40	3.22	0.00	0.89	-0.33	0.05	0.00	0.00	0.18	-0.13	-0.38	2.83	2.32	-0.55	-0.40	3.40	-0.13	0.50
20	MRI-ESM2-0	3.12	1.64	-0.35	-0.40	2.39	0.00	1.48	-1.20	-3.49	0.00	0.00	0.08	-3.57	2.29	1.92	-1.85	-0.35	-0.40	2.48	-3.57	3.76
21	NESM3	4.34	3.77	-0.53	-0.99	5.29	0.00	0.57	-0.71	0.04	0.00	0.00	0.29	-0.25	-0.75	3.63	3.81	-0.53	-0.99	5.58	-0.25	-0.18
22	NorCPM1	1.73	5.27	0.08	2.12	3.07	0.00	-3.54	3.87	1.01	0.00	0.00	0.13	0.87	2.86	5.59	6.28	0.08	2.12	3.20	0.87	-0.69
23	SAM0-UNICON	4.77	4.27	0.22	1.73	2.31	0.00	0.50	3.38	0.84	0.00	0.00	0.14	0.70	2.54	8.15	5.11	0.22	1.73	2.45	0.70	3.04
24	UKESM1-0-LL	3.03	1.48	-0.54	0.63	1.39	0.00	1.55	-0.98	-1.40	0.00	0.00	-0.02	-1.38	0.43	2.05	0.08	-0.54	0.63	1.37	-1.38	1.97
	multi-model mean	3.99	3.00	-0.26	1.62	1.64	0.00	0.98	0.98	0.45	0.00	0.00	0.09	0.37	0.53	4.97	3.46	-0.26	1.62	1.73	0.37	1.51

Table S3. The standard deviation (STD) of the biases in the global mean radiation fluxes of all the models examined.

			overall radiation biases			
CMIP6 model bias	2.93	3.71	2.24	2.46	2.35	3.96
			kernel-diagnosed component radiation biases			
total bias	3.10	3.07	2.82	2.40	2.20	3.91
surface (land) temperature	0.26	---	0.26	0.37	---	0.37
atmospheric temperature	1.98	---	1.98	1.83	---	1.83
water vapor	1.51	0.19	1.69	1.92	0.11	2.02
surface albedo		1.69	1.69	---	2.17	2.17
cloud	2.55	3.96	2.76	---	---	---
residual	1.96	1.78	2.45	1.96	1.78	2.45

Table S4. The spatial correlation (cor) between the globally distributed component and total radiation biases in all-sky.

		LW									SW									Net							
Model #	Model name	dR	sumdR	dRts	dRta	dRq	dRalb	dRc	dCRE	res	dR	sumdR	dRts	dRta	dRq	dRalb	dRc	dCRE	res	dR	sumdR	dRts	dRta	dRq	dRalb	dRc	dCRE	res
1	ACCESS-CM2	1.00	0.95	0.24	0.45	0.49	0.00	0.93	0.90	-0.02	1.00	0.75	0.00	0.00	-0.15	0.20	0.79	0.72	0.02	1.00	0.74	0.24	0.45	0.20	0.20	0.66	0.59	-0.01
2	BCC-ESM1	1.00	0.94	0.26	0.20	0.46	0.00	0.88	0.83	-0.10	1.00	0.87	0.00	0.00	0.01	0.36	0.84	0.79	-0.10	1.00	0.85	0.26	0.20	0.22	0.36	0.72	0.63	-0.15
3	CanESM5	1.00	0.92	0.20	0.16	0.57	0.00	0.87	0.82	-0.06	1.00	0.77	0.00	0.00	-0.13	0.30	0.73	0.65	0.05	1.00	0.74	0.20	0.16	0.21	0.30	0.69	0.63	0.08
4	CAS-ESM2-0	1.00	0.96	0.11	0.16	0.64	0.00	0.91	0.90	0.07	1.00	0.91	0.00	0.00	0.29	0.32	0.88	0.85	-0.11	1.00	0.86	0.11	0.16	-0.05	0.32	0.85	0.80	-0.10
5	CESM2	1.00	0.91	0.19	0.17	0.51	0.00	0.88	0.86	-0.07	1.00	0.76	0.00	0.00	-0.19	0.19	0.85	0.82	0.00	1.00	0.75	0.19	0.17	0.07	0.19	0.80	0.76	-0.06
6	CIESM	1.00	0.88	0.32	0.34	0.20	0.00	0.82	0.79	0.01	1.00	0.85	0.00	0.00	0.34	0.09	0.91	0.90	0.05	1.00	0.86	0.32	0.34	-0.15	0.09	0.92	0.89	-0.04
7	CMCC-CM2-SR5	1.00	0.87	0.22	0.15	0.29	0.00	0.86	0.82	0.02	1.00	0.84	0.00	0.00	0.21	0.35	0.88	0.81	-0.09	1.00	0.86	0.22	0.15	-0.05	0.35	0.86	0.73	-0.22
8	CNRM-ESM2-1	1.00	0.92	0.17	0.12	0.68	0.00	0.84	0.81	-0.02	1.00	0.82	0.00	0.00	0.04	0.20	0.81	0.78	0.12	1.00	0.80	0.17	0.12	0.19	0.20	0.77	0.74	0.10
9	E3SM-1-0	1.00	0.90	0.19	-0.02	0.66	0.00	0.85	0.81	-0.09	1.00	0.77	0.00	0.00	-0.03	0.21	0.83	0.79	-0.01	1.00	0.76	0.19	-0.02	0.13	0.21	0.81	0.77	-0.04
10	EC-Earth3	1.00	0.77	-0.11	0.15	0.63	0.00	0.79	0.83	0.28	1.00	0.81	0.00	0.00	0.11	0.29	0.80	0.73	0.12	1.00	0.82	-0.11	0.15	0.36	0.29	0.85	0.80	0.16
11	FGOALS-g3	1.00	0.94	0.28	0.16	0.63	0.00	0.89	0.77	0.03	1.00	0.79	0.00	0.00	0.00	0.19	0.79	0.74	0.10	1.00	0.81	0.28	0.16	0.29	0.19	0.81	0.76	0.04
12	GFDL-CM4	1.00	0.83	0.23	0.05	0.62	0.00	0.84	0.79	-0.04	1.00	0.68	0.00	0.00	-0.08	0.24	0.71	0.66	0.04	1.00	0.66	0.23	0.05	0.20	0.24	0.67	0.61	0.03
13	GISS-E2-2-G	1.00	0.84	0.28	0.02	0.56	0.00	0.78	0.71	-0.05	1.00	0.75	0.00	0.00	-0.08	0.31	0.72	0.68	0.03	1.00	0.78	0.28	0.02	0.32	0.31	0.69	0.64	0.05
14	HadGEM3-GC31-LL	1.00	0.95	0.18	0.43	0.46	0.00	0.95	0.94	-0.14	1.00	0.73	0.00	0.00	-0.16	0.14	0.81	0.76	0.03	1.00	0.77	0.18	0.43	0.11	0.14	0.70	0.63	-0.09
15	IITM-ESM	1.00	0.96	0.25	0.05	0.66	0.00	0.94	0.91	-0.11	1.00	0.94	0.00	0.00	0.26	0.34	0.89	0.86	-0.15	1.00	0.94	0.25	0.05	0.23	0.34	0.87	0.84	-0.14
16	INM-CM5-0	1.00	0.95	0.42	0.41	0.24	0.00	0.93	0.89	-0.08	1.00	0.80	0.00	0.00	-0.07	0.43	0.75	0.69	-0.04	1.00	0.84	0.42	0.41	-0.18	0.43	0.76	0.69	-0.10
17	IPSL-CM6A-LR	1.00	0.89	0.01	0.36	0.55	0.00	0.76	0.74	0.20	1.00	0.77	0.00	0.00	-0.12	0.21	0.79	0.76	0.14	1.00	0.74	0.01	0.36	0.19	0.21	0.75	0.73	0.14
18	MIROC-ES2L	1.00	0.95	0.53	0.08	0.70	0.00	0.82	0.71	0.03	1.00	0.93	0.00	0.00	0.40	0.46	0.88	0.84	-0.25	1.00	0.90	0.53	0.08	-0.05	0.46	0.88	0.86	-0.20
19	MPI-ESM1-2-LR	1.00	0.94	0.08	0.27	0.50	0.00	0.92	0.89	-0.12	1.00	0.82	0.00	0.00	-0.22	0.21	0.86	0.81	-0.03	1.00	0.79	0.08	0.27	0.19	0.21	0.79	0.74	-0.06
20	MRI-ESM2-0	1.00	0.86	0.14	-0.11	0.53	0.00	0.85	0.81	0.04	1.00	0.72	0.00	0.00	-0.19	0.45	0.53	0.36	0.05	1.00	0.72	0.14	-0.11	0.24	0.45	0.39	0.17	0.05
21	NESM3	1.00	0.96	0.12	-0.04	0.75	0.00	0.93	0.92	-0.15	1.00	0.84	0.00	0.00	-0.01	0.23	0.88	0.84	-0.10	1.00	0.79	0.12	-0.04	0.38	0.23	0.73	0.67	-0.02
22	NorCPM1	1.00	0.93	0.23	0.26	0.34	0.00	0.89	0.88	-0.12	1.00	0.86	0.00	0.00	-0.08	0.15	0.90	0.88	-0.12	1.00	0.82	0.23	0.26	-0.24	0.15	0.85	0.82	-0.03
23	SAM0-UNICON	1.00	0.90	0.37	0.37	0.09	0.00	0.81	0.72	0.02	1.00	0.71	0.00	0.00	-0.04	0.17	0.76	0.73	0.05	1.00	0.78	0.37	0.37	0.12	0.17	0.83	0.80	-0.12
24	UKESM1-0-LL	1.00	0.95	0.27	0.46	0.43	0.00	0.95	0.93	-0.23	1.00	0.73	0.00	0.00	-0.16	0.15	0.80	0.75	0.03	1.00	0.76	0.27	0.46	0.13	0.15	0.70	0.61	-0.16
	multi-model mean	1.00	0.84	0.16	0.17	0.55	0.00	0.83	0.80	-0.05	1.00	0.69	0.00	0.00	0.04	0.15	0.80	0.79	-0.03	1.00	0.70	0.09	0.16	-0.06	0.12	0.78	0.77	-0.06

Table S5. The spatial correlation (cor) between the globally distributed component and total radiation biases in clear-sky.

		LW							SW						Net					
Model #	Model name	dR	sum(dRx)	dRts	dRta	dRq	dRalb	res	dR	sum(dRx)	dRts	dRta	dRq	dRalb	res	dR	sum(dRx)	dRts	dRta	dRq	dRalb	res
1	ACCESS-CM2	1.00	0.78	0.45	0.23	0.61	0.00	0.21	1.00	0.56	0.00	0.00	0.11	0.56	0.21	1.00	0.61	0.45	0.23	0.41	0.56	0.28
2	BCC-ESM1	1.00	0.81	0.59	0.25	0.43	0.00	0.08	1.00	0.71	0.00	0.00	0.13	0.70	0.05	1.00	0.77	0.59	0.25	0.51	0.70	0.00
3	CanESM5	1.00	0.77	0.60	0.43	0.17	0.00	0.12	1.00	0.64	0.00	0.00	0.11	0.63	0.24	1.00	0.63	0.60	0.43	0.26	0.63	0.25
4	CAS-ESM2-0	1.00	0.81	0.49	0.36	0.49	0.00	0.23	1.00	0.73	0.00	0.00	0.61	0.73	-0.01	1.00	0.70	0.49	0.36	0.19	0.73	0.03
5	CESM2	1.00	0.63	0.40	0.37	0.29	0.00	0.29	1.00	0.32	0.00	0.00	-0.08	0.32	0.41	1.00	0.39	0.40	0.37	0.23	0.32	0.36
6	CIESM	1.00	0.70	0.53	0.50	0.02	0.00	0.19	1.00	0.33	0.00	0.00	0.05	0.33	0.43	1.00	0.41	0.53	0.50	0.34	0.33	0.38
7	CMCC-CM2-SR5	1.00	0.61	0.47	0.35	0.16	0.00	0.26	1.00	0.55	0.00	0.00	0.33	0.55	0.19	1.00	0.68	0.47	0.35	0.06	0.55	0.06
8	CNRM-ESM2-1	1.00	0.72	0.39	0.31	0.41	0.00	0.39	1.00	0.51	0.00	0.00	0.20	0.50	0.51	1.00	0.55	0.39	0.31	0.20	0.50	0.49
9	E3SM-1-0	1.00	0.69	0.54	0.43	0.31	0.00	0.27	1.00	0.48	0.00	0.00	0.35	0.47	0.28	1.00	0.46	0.54	0.43	0.23	0.47	0.29
10	EC-Earth3	1.00	0.13	-0.07	0.30	0.22	0.00	0.71	1.00	0.58	0.00	0.00	0.35	0.57	0.41	1.00	0.56	-0.07	0.30	0.34	0.57	0.31
11	FGOALS-g3	1.00	0.84	0.72	0.29	0.29	0.00	0.29	1.00	0.60	0.00	0.00	0.29	0.59	0.35	1.00	0.58	0.72	0.29	0.29	0.59	0.27
12	GFDL-CM4	1.00	0.55	0.43	0.21	0.35	0.00	0.27	1.00	0.42	0.00	0.00	0.21	0.42	0.39	1.00	0.38	0.43	0.21	0.30	0.42	0.45
13	GISS-E2-2-G	1.00	0.52	0.51	-0.16	0.25	0.00	0.61	1.00	0.47	0.00	0.00	0.06	0.46	0.50	1.00	0.57	0.51	-0.16	0.09	0.46	0.47
14	HadGEM3-GC31-LL	1.00	0.70	0.37	0.26	0.56	0.00	0.09	1.00	0.49	0.00	0.00	0.14	0.49	0.27	1.00	0.61	0.37	0.26	0.41	0.49	0.25
15	IITM-ESM	1.00	0.80	0.55	0.23	0.53	0.00	0.05	1.00	0.79	0.00	0.00	0.35	0.79	0.06	1.00	0.79	0.55	0.23	0.23	0.79	0.11
16	INM-CM5-0	1.00	0.82	0.62	0.54	0.35	0.00	0.06	1.00	0.61	0.00	0.00	0.17	0.62	0.22	1.00	0.67	0.62	0.54	0.10	0.62	0.24
17	IPSL-CM6A-LR	1.00	0.73	0.27	0.53	0.49	0.00	0.48	1.00	0.38	0.00	0.00	0.31	0.37	0.59	1.00	0.39	0.27	0.53	0.45	0.37	0.59
18	MIROC-ES2L	1.00	0.89	0.80	0.17	0.45	0.00	0.28	1.00	0.78	0.00	0.00	0.50	0.78	-0.04	1.00	0.63	0.80	0.17	0.22	0.78	0.22
19	MPI-ESM1-2-LR	1.00	0.72	0.44	0.18	0.49	0.00	0.18	1.00	0.53	0.00	0.00	0.09	0.53	0.26	1.00	0.55	0.44	0.18	0.34	0.53	0.32
20	MRI-ESM2-0	1.00	0.53	0.35	0.02	0.40	0.00	0.47	1.00	0.73	0.00	0.00	-0.14	0.73	0.22	1.00	0.77	0.35	0.02	0.39	0.73	0.25
21	NESM3	1.00	0.80	0.38	0.06	0.66	0.00	0.09	1.00	0.51	0.00	0.00	0.10	0.52	0.26	1.00	0.60	0.38	0.06	0.50	0.52	0.31
22	NorCPM1	1.00	0.70	0.55	0.52	0.01	0.00	0.21	1.00	0.39	0.00	0.00	0.11	0.39	0.44	1.00	0.49	0.55	0.52	0.32	0.39	0.37
23	SAM0-UNICON	1.00	0.81	0.69	0.78	-0.13	0.00	0.14	1.00	0.34	0.00	0.00	-0.37	0.36	0.53	1.00	0.34	0.69	0.78	0.20	0.36	0.39
24	UKESM1-0-LL	1.00	0.70	0.42	0.20	0.55	0.00	0.05	1.00	0.51	0.00	0.00	0.11	0.51	0.22	1.00	0.61	0.42	0.20	0.44	0.51	0.19
	multi-model mean	1.00	0.53	0.29	0.23	0.41	0.00	0.31	1.00	0.24	0.00	0.00	0.02	0.25	0.43	1.00	0.28	-0.02	-0.05	0.30	0.20	0.45

Table S6. The root-mean-square of the biases at every grid point acroass the globe in each model. Units: W m-2.

		all-sky			clear-sky		
Model #	Model name	LW	SW	Net	LW	SW	Net
1	ACCESS-CM2	8.60	9.06	7.51	4.11	5.16	6.36
2	BCC-ESM1	11.15	15.48	10.42	6.06	8.09	11.49
3	CanESM5	7.09	9.86	8.95	3.76	7.38	7.45
4	CAS-ESM2-0	10.90	16.76	14.81	9.34	9.10	16.31
5	CESM2	6.21	9.26	8.03	5.13	5.32	8.70
6	CIESM	5.67	12.30	11.19	7.62	4.89	8.80
7	CMCC-CM2-SR	5.20	10.73	9.89	6.44	6.68	11.57
8	CNRM-ESM2-1	6.94	12.44	10.88	6.33	7.07	9.34
9	E3SM-1-0	5.35	9.36	7.97	3.66	5.79	7.06
10	EC-Earth3	5.23	10.73	11.24	2.61	7.35	6.73
11	FGOALS-g3	9.84	11.80	10.46	5.80	7.05	6.57
12	GFDL-CM4	4.63	7.81	7.10	4.34	5.85	7.69
13	GISS-E2-2-G	9.04	14.25	12.60	9.11	9.12	11.70
14	HadGEM3-GC3	8.43	8.86	7.50	3.89	5.36	6.27
15	IITM-ESM	11.33	23.54	20.05	4.21	9.41	9.13
16	INM-CM5-0	8.71	12.70	11.86	4.16	9.68	9.15
17	IPSL-CM6A-LR	6.22	11.30	9.93	4.85	7.26	8.61
18	MIROC-ES2L	13.82	20.89	15.21	10.26	8.14	13.54
19	MPI-ESM1-2-L	7.80	11.36	8.69	4.33	5.56	6.16
20	MRI-ESM2-0	5.04	8.10	7.52	3.96	8.96	9.36
21	NESM3	10.62	12.33	8.69	5.71	5.49	7.10
22	NorCPM1	9.37	14.84	10.41	3.59	6.92	8.12
23	SAM0-UNICON	6.09	8.42	8.52	5.71	6.24	9.36
24	UKESM1-0-LL	8.10	8.83	7.31	4.13	5.51	6.53
	multi-model me	4.90	7.45	6.41	4.55	4.58	6.66